

1 **Organic geochemistry of the early Toarcian oceanic anoxic event in Hawsker**

2 **Bottoms, Yorkshire, England**

3

4 K. L. French<sup>a\*</sup>, J. Sepúlveda<sup>b</sup>, J. Trabucho-Alexandre<sup>c</sup>, D. R. Gröcke<sup>c</sup>, R. E. Summons<sup>b</sup>

5

6 <sup>a</sup> Joint Program in Chemical Oceanography; Massachusetts Institute of Technology and

7 Woods Hole Oceanographic Institution, Cambridge, MA 02139, United States

8 <sup>b</sup> Department of Earth, Atmospheric, and Planetary Sciences; Massachusetts Institute of

9 Technology, Cambridge, MA 02139, United States

10 <sup>c</sup> Department of Earth Sciences, University of Durham, Durham, DH1 3LE, UK

11

12 \*Corresponding author:

13 E-mail address: [klfrench@mit.edu](mailto:klfrench@mit.edu) (K. L. French)

14 Tel: +01 617-324-3953

15 **Abstract**

16 A comprehensive organic geochemical investigation of the Hawsker Bottoms  
17 outcrop section in Yorkshire, England has provided new insights about environmental  
18 conditions leading into and during the Toarcian oceanic anoxic event (T-OAE; ~183 Ma).  
19 Rock-Eval and molecular analyses demonstrate that the section is uniformly within the  
20 early oil window. Hydrogen index (HI), organic petrography, polycyclic aromatic  
21 hydrocarbon (PAH) distributions, and tricyclic terpane ratios mark a shift to a lower  
22 relative abundance of terrigenous organic matter supplied to the sampling locality during  
23 the onset of the T-OAE and across a lithological transition. Unlike other ancient intervals  
24 of anoxia and extinction, biomarker indices of planktonic community structure do not  
25 display major changes or anomalous values. Depositional environment and redox  
26 indicators support a shift towards more reducing conditions in the sediment porewaters  
27 and the development of a seasonally stratified water column during the T-OAE. In  
28 addition to carotenoid biomarkers for green sulfur bacteria (GSB), we report the first  
29 occurrence of okenane, a marker of purple sulfur bacteria (PSB), in marine samples  
30 younger than ~1.64 Ga. Based on modern observations, a planktonic source of okenane's  
31 precursor, okenone, would require extremely shallow photic zone euxinia (PZE) and a  
32 highly restricted depositional environment. However, due to coastal vertical mixing, the  
33 lack of planktonic okenone production in modern marine sulfidic environments, and  
34 building evidence of okenone production in mat-dwelling Chromatiaceae, we propose a  
35 sedimentary source of okenone as an alternative. Lastly, we report the first parallel  
36 compound-specific  $\delta^{13}\text{C}$  record in marine- and terrestrial-derived biomarkers across the  
37 T-OAE. The  $\delta^{13}\text{C}$  records of short-chain *n*-alkanes, acyclic isoprenoids, and long-chain *n*-

38 alkanes all encode negative carbon isotope excursions (CIEs), and together, they support  
39 an injection of isotopically light carbon that impacted both the atmospheric and marine  
40 carbon reservoirs. To date, molecular  $\delta^{13}\text{C}$  records of the T-OAE display a negative CIE  
41 that is smaller in magnitude compared to the bulk organic  $\delta^{13}\text{C}$  excursion. Although  
42 multiple mechanisms could explain this observation, our molecular, petrographic, and  
43 Rock-Eval data suggest that variable mixing of terrigenous and marine organic matter is  
44 an important factor affecting the bulk organic  $\delta^{13}\text{C}$  records of the T-OAE.

45

46 Keywords: Toarcian oceanic anoxic event; lipid biomarkers; okenane; photic zone  
47 euxinia, stable carbon isotopes; Hawsker Bottoms

## 48 **1. Introduction**

49

50           Several transient episodes of enhanced deposition and preservation of organic-  
51 rich sediments punctuated the Mesozoic Era. A combination of factors may have caused  
52 these intervals, known as oceanic anoxic events (OAEs), including greenhouse conditions  
53 and enhanced marine productivity (e.g. Schlanger and Jenkyns, 1976; Jenkyns, 1980;  
54 1988; 2010; Trabucho-Alexandre et al., 2010). The first Mesozoic OAE was the Early  
55 Jurassic Toarcian OAE (T-OAE; ~183 Ma), which was associated with elevated  
56 extinction rates, enhanced weathering rates, warm temperatures, ocean acidification, and  
57 a negative carbon isotope excursion (CIE) (Hesselbo et al., 2000; Cohen et al., 2004;  
58 Bambach, 2006; Hesselbo et al., 2007; Jenkyns, 2010; Kiessling and Simpson, 2011).  
59 The duration of the T-OAE is not precisely known but may have lasted on the order of  
60 several hundred thousand years (Kemp et al., 2005; Suan et al., 2008; Kemp et al., 2011).  
61 The Karoo and Ferrar igneous provinces, which erupted at  $183 \pm 1$  Ma, may have  
62 coincided with the Pliensbachian-Toarcian extinction (Pálffy and Smith, 2000; Courtillot  
63 and Renne, 2003). However, better radiometric dating of the volcanism and OAE are  
64 required to confidently link these two events. Although multiple mechanisms have been  
65 proposed to account for the Toarcian negative CIE, including methane hydrate  
66 dissociation, upwelling of isotopically light waters, thermogenic release of methane, and  
67 biomass burning (Hesselbo et al., 2000; Schouten et al., 2000; McElwain et al., 2005; van  
68 de Schootbrugge et al., 2005; Finkelstein et al., 2006), the source of the isotopically light  
69 carbon remains unclear.

70           The analysis of sedimentary organic matter provides the opportunity to evaluate  
71 environmental and ecological responses to carbon cycle perturbations, as well as  
72 potentially constraining the perturbation itself. Previous organic geochemical work across  
73 the T-OAE has indicated changes in planktonic community structure and redox  
74 chemistry, particularly the development of photic zone euxinia (PZE) (e.g. Farrimond et  
75 al., 1989; 1994; Schouten et al., 2000; Pancost et al., 2004; Schwark and Frimmel, 2004;  
76 Bowden et al., 2006; van Breugel et al., 2006). However, since biomarker records can  
77 reflect local responses, additional comprehensive organic geochemical studies from  
78 multiple locations are required to build a global perspective of ecological and  
79 environmental change associated with the T-OAE. Here, we investigate the temporal  
80 variation of lipid biomarkers, Rock-Eval data, organic petrography, and compound-  
81 specific carbon isotopes from the Lower Jurassic section at Hawsker Bottoms, Yorkshire,  
82 England.

83

## 84 **2. Geologic Setting and Site Description of Hawsker Bottoms, Yorkshire, England**

85

86           A well-studied section of the Toarcian OAE is located on the Yorkshire coast in  
87 northern England. We analyzed sample splits spanning 14 m of an organic-rich, lower  
88 Jurassic outcrop section in the Cleveland Basin at Hawsker Bottoms previously studied  
89 by Hesselbo et al. (2000). The lithology is dominated by black shales containing discrete  
90 levels of calcite concretions and constitutes the Jet Rock *sensu stricto* (Hesselbo and  
91 Jenkyns, 1995). The sections around Hawsker Bottoms have been used for defining the  
92 ammonite biostratigraphy of the Toarcian (Howarth, 1992).

93           The Early Jurassic paleogeography of the area, although somewhat uncertain, is  
94 depicted in published paleogeographic maps (e.g. Bradshaw et al., 1992). The Cleveland  
95 Basin of North Yorkshire was part of a system of shallow epicontinental seas and small  
96 extensional tectonic basins linked to the Central Graben via the Sole Pit Basin. The  
97 region formed part of the broad epicontinental sea that covered much of northwest  
98 Europe. Marine sedimentation was initiated during the Late Triassic, and a succession of  
99 marine siliciclastic mudstones accumulated during the Early Jurassic.

100           The Grey Shale Member of the Whitby Mudstone Formation consists of  
101 bioturbated, silty mudstones with beds of calcareous siderite concretions. The mudstones  
102 have thin sharp-based beds, wave ripple, and starved ripple laminations (Wignall et al.,  
103 2005; Ghadeer and Macquaker, 2011). Grain size and bioturbation intensity decrease  
104 toward the top of the unit, and sediment color darkens. The Jet Rock Member consists of  
105 dark, organic matter-rich, fissile mudstones with abundant ammonites and horizons of  
106 calcareous nodules. The boundary between these two members of the Whitby Mudstone  
107 Formation likely represents an increase in water depth in the basin.

108           The early Toarcian (*D. tenuicostatum* Zone) was a period of major basin  
109 subsidence throughout England. Organic matter content fluctuates through the Grey  
110 Shales, but increasing levels of organic matter are present from the *D. semicelatum*  
111 Subzone to the *C. exaratum* Subzone (*H. falciferum* Zone). Minor shoaling cycles with  
112 striped siltstone laminae suggest that water depths were on the order of tens of meters  
113 (Powell, 2010). Similarly, sedimentary structures suggest deposition during storms by the  
114 effects of waves (Wignall et al., 2005; Ghadeer and Macquaker, 2011). Thus, bottom  
115 water conditions were more energetic than is commonly thought, where the water column

116 was likely shallower than 50 m. Consequently, Hawsker Bottoms likely represents an  
117 inner continental shelf environment, which physical oceanographers define as the region  
118 where turbulence from the surface and bottom boundary layers effectively homogenizes  
119 the whole water column (Lentz and Fewings, 2012). Accordingly, inner shelf  
120 environments are typically a few meters to tens of meters deep

121         The abundance of ammonites in the shales indicates that the water column was at  
122 times oxygenated and favorable to nektonic faunas (Powell, 2010). The abundance of thin  
123 beds with tops homogenized by bioturbation suggests that long-term, persistent bottom  
124 water anoxia did not occur in the basin (Ghadeer and Macquaker, 2011). Besides  
125 deposition as bedload by geostrophic flows and density currents, additional sediment was  
126 supplied by suspension settling. Textural analyses have shown that much of the  
127 sedimentary organic matter was delivered to the seafloor as fecal pellets, flocs, or other  
128 organo-mineralic aggregates (Ghadeer and Macquaker, 2011). The contribution of a  
129 biogenic component to rock composition varies, and the differences have been attributed  
130 to a changing balance of primary production relative to dilution and length of transport  
131 path during deposition (Macquaker and Taylor, 1996; Wignall et al., 2005; Ghadeer and  
132 Macquaker, 2011).

133

### 134 **3. Methods**

135         Powdered rock samples were analyzed by Rock-Eval pyrolysis. The total organic  
136 carbon (TOC; %),  $T_{\max}$  (°C),  $S_1$ , and  $S_2$  were determined and used to calculate the  
137 hydrogen index (HI) and production index (PI). Kerogen isolates from four samples  
138 across the section were mounted onto slides in duplicate and assessed optically under

139 white light and fluorescent light using a Zeiss research microscope and a Zeiss x 40  
140 Plank-Neofluar objective. A Zeiss Axioskop, Axio Image D1, and a Zeiss 18 filter set  
141 were used to take photomicrographs and fluorescence images.

142 Powdered samples (~ 5 g) were extracted using a Dionex ASE 200 Accelerated  
143 Solvent Extractor with a solvent mixture of dichloromethane:methanol 9:1 (v/v).  
144 Elemental sulfur was removed from the total lipid extract (TLE). Asphaltenes were  
145 separated from the maltene fraction, which was then separated into saturated, aromatic,  
146 and polar fractions by silica gel chromatography. The saturated and aromatic fractions  
147 were analyzed by gas chromatography-mass spectrometry (GC-MS) and gas  
148 chromatography-metastable reaction monitoring-mass spectrometry (GC-MRM-MS).  
149 Carbon isotopic measurements of saturated hydrocarbons were made by gas  
150 chromatography/combustion/ isotope ratio mass spectrometry (GC-C-IRMS) using a  
151 ThermoFinnigan Delta Plus XP coupled to a ThermoFinnigan Trace GC. The mean value  
152 of triplicate analyses are reported here in per mil (‰) relative to Vienna Pee Dee  
153 belemnite (VPDB), and the standard deviation from the mean value was 0.4‰ or less. A  
154 detailed description of methods is included in the supplementary online material (SOM).  
155

## 156 **4. Results and Discussion**

### 157 *4.1 Rock-Eval analysis*

158 Rock-Eval results provided insight into the thermal maturity and type of organic  
159 matter preserved in the Hawsker Bottoms sediments. The TOC percentage (Hesselbo et  
160 al., 2000) was plotted for comparison with the HI, PI, and  $T_{\max}$  (fig. 1). The narrow range  
161 of the PI (0.11-0.18) and  $T_{\max}$  (429-440°C) parameters indicate that thermal maturity is



162 uniform through the section and at the early stage of oil generation (Peters et al., 2005).  
163 Molecular indices of thermal maturity further substantiate this conclusion (see section  
164 4.2).

165         The HI data reveal that the type of organic matter undergoes a transition that  
166 appears to coincide with a lithological transition from medium grey shale to dark grey  
167 thin-bedded shale within the limitations of our sampling resolution. The low HI values  
168 below -2.5 m are characteristic of type III kerogen, whereas the higher HI values above -  
169 3 m are characteristic of type II kerogen (Peters et al., 2005). Type III kerogen is  
170 dominated by either terrigenous or highly degraded organic matter, and type II kerogen is  
171 typically derived from marine organic matter (Peters et al., 2005).

172         Published HI values from other T-OAE localities also increase across the  
173 initiation of the CIE (Prauss et al., 1991; Schouten et al., 2000; Röhl et al., 2001;  
174 Sabatino et al., 2009; Suan et al., 2011). Previous workers have attributed the HI  
175 variability to different degrees of organic matter degradation under varying redox  
176 conditions (Schouten et al., 2000; Röhl et al., 2001; Sabatino et al., 2009). Alternatively,  
177 others have argued that the HI variability represents a shift in the composition of the  
178 organic matter (Suan et al., 2011). Petrographic and molecular evidence for the presence  
179 of plant-derived material in these sediments (see section 4.3) supports the conclusion that  
180 lower HI values at the bottom of the section are due to a larger abundance of terrigenous  
181 organic matter relative to marine organic matter.

182

183 *4.2 Molecular indicators of thermal maturity*

184 The thermal history of the section was further assessed according to molecular  
185 thermal maturity parameters (fig. 2). The C<sub>31</sub> hopane 22S/(22S+22R) ratio was constant  
186 through the section and exhibited a narrow range between 0.58 and 0.59. A value of  
187 ~0.55 represents the endpoint which is reached around the main phase of oil generation  
188 (Peters et al., 2005). The C<sub>30</sub> hopane  $\beta\alpha/(\beta\alpha+\alpha\beta)$  ratio ranged from 0.08 to 0.11, which is  
189 close to values indicative of a mature source rock (Peters et al., 2005). The C<sub>29</sub> sterane  
190  $\alpha\alpha\alpha$  20S/(20S+20R) ratio varied from 0.52 to 0.57, which is comparable to the endpoint  
191 value of 0.52-0.55 (Peters et al., 2005). In summary, molecular thermal maturity  
192 indicators corroborate the Rock-Eval results, further supporting a uniform thermal  
193 maturity within the early window of oil generation.

194 Some biomarker-based thermal maturity parameters can be influenced by  
195 additional factors such as source and diagenetic effects (Moldowan et al., 1986; Dahl et  
196 al., 1993; Peters et al., 2005; Bennett and Olsen, 2007; French et al., 2012). Indeed, two  
197 of the thermal maturity parameters presented in figure 2 exhibit some variation tracking  
198 changes in lithology and source input, despite the multiple lines of evidence supporting  
199 constant thermal maturity through the section. The Ts/(Ts+Tm) ratio, where Tm is C<sub>27</sub> 17  
200  $\alpha$ -trisorhopane and Ts is C<sub>27</sub> 18  $\alpha$ -trisorhopane, varied from 0.41 to 0.59, whereas the  
201 diasterane/sterane ratio of C<sub>27-29</sub> compounds ranged from 1.08 to 1.44. Both ratios deviate  
202 from a relatively constant pattern in the lower ~2 meters of the section. This pattern is  
203 explained by changes in lithology and/or organic matter source input, which is consistent  
204 with lower HI values and additional evidence supporting variable terrigenous organic  
205 input (see section 4.3).

206

### 207 4.3 Biomarker and petrographic evidence of terrigenous organic matter input

208 A combination of molecular and petrographic analyses was performed to evaluate  
209 the relative contribution of terrigenous organic matter through the sampling interval (fig.  
210 3). Previous work has suggested a terrigenous source for C<sub>19</sub> and C<sub>20</sub> tricyclic terpanes,  
211 which has led to the use of C<sub>19</sub>/C<sub>23</sub> and C<sub>20</sub>/C<sub>23</sub> tricyclic terpane ratios to identify input of  
212 terrigenous organic matter (Noble et al., 1986; Peters et al., 2005). These two ratios  
213 display higher values in the lowest part of the section and decrease after the lithological  
214 transition at -2.5 meters, indicating relatively greater terrigenous organic matter input in  
215 the lowermost part of the sampling interval.

216 A wide range of PAHs was detected in the Hawsker Bottoms samples, including  
217 phenanthrene, fluoranthene, pyrene, benzo[a]anthracene, triphenylene, chrysene,  
218 benzo[b]fluoranthene, benzo[k]fluoranthene, benzo[e]pyrene, indeno[c,d]pyrene,  
219 dibenzo[a,h]anthracene, benzo[g,h,i]perylene, coronene, and retene. PAHs are a diverse  
220 set of compounds with multiple documented sources including products of pyrolysis,  
221 combustion, hydrothermal activity, and igneous intrusion as well as direct inputs from  
222 algae, fungi, vascular plants, and extraterrestrial organics (Kawka and Simoneit, 1990;  
223 George, 1992; Jiang et al., 2000; Sephton et al., 2005; Grice et al., 2007; Marynowski and  
224 Simoneit, 2009). PAHs have been used to reconstruct the history of wildfires, higher  
225 plant input, and anthropogenic activity, where peri-condensed, unsubstituted PAHs are  
226 markers for combustion of organic matter (Hites et al., 1977; Venkatesan and Dahl, 1989;  
227 Killops and Massoud, 1992; Kruge et al., 1994; Jiang et al., 1998; Arinobu et al., 1999;  
228 Finkelstein et al., 2005; Peters et al., 2005; Marynowski and Simoneit, 2009). Some  
229 sedimentary PAHs, such as phenanthrene, chrysene, and triphenylene, are more affected

230 by diagenesis or additional sources (Jiang et al., 1998; Grice et al., 2007), so they were  
231 not included in the total PAH sum plotted in figure 3b. Although the patterns are not  
232 identical, enhanced concentrations of total PAH co-occur with elevated  $C_{19}/C_{23}$  and  
233  $C_{20}/C_{23}$  tricyclic terpane ratios in the bottom 2 meters of the sampling interval. Some  
234 PAHS, such as retene, are thought to derive from higher plants, in particular coniferous  
235 resin (Wakeham et al., 1980; Ellis et al., 1996; Jiang et al., 1998; Grice et al., 2005;  
236 Peters et al., 2005), although algal and bacterial sources have been reported as well (Wen  
237 et al., 2000). Retene was detected in all samples, and its concentration was plotted  
238 separately as a marker of higher plant input in figure 3c. Retene was more abundant in  
239 the lowest interval of the section, which is consistent with the total PAHs, tricyclic  
240 terpane ratios, and HI data.

241         Microscopic analysis of four kerogen samples adds an additional line of evidence  
242 supporting stratigraphic variations in kerogen type and organic matter sources. According  
243 to the petrographic results, the kerogen is comprised of as much as 80% of terrigenous  
244 organic matter in the bottom of the section and about 25-40% in the remainder of the  
245 sampling interval (fig. 3d). Since the elemental, molecular, and isotopic composition of  
246 organic matter from higher plants is distinct from marine organic matter, HI can reflect  
247 the compositional difference of distinct types of organic matter (e.g. Talbot and  
248 Livingstone, 1989). Assuming constant HI values for terrigenous and marine organic  
249 matter end-members, the percent terrigenous organic matter was estimated through the  
250 section using the linear relationship between the percent terrigenous macerals measured  
251 by optical microscopy and the corresponding HI (see SOM for more details). Calculated

252 values of  $f_{Terr\ OM}$  ranged from 12 to 85%, where the highest values were found in the  
253 lowermost part of the section (fig. 3e).

254 The stratigraphic change in the relative supply of terrigenous organic matter ,  
255 which is supported by the HI, molecular, and petrographic results, may have been driven  
256 by effects related to rising sea level (Hesselbo, 2008; Suan et al., 2011). Considering that  
257 increased rates of continental weathering across the T-OAE would have enhanced  
258 delivery of terrigenous material (Cohen et al., 2004), the opposite trend recorded in our  
259 data might be best explained by progressive remoteness from the coastline on a gently  
260 sloping shelf during sea level transgression (e.g. Macquaker et al., 2010). However, sea  
261 level related effects might not be the only factor responsible for the changing signal in  
262 relative abundance of terrigenous and marine organic matter. For example, enhanced  
263 marine export productivity and/or enhanced marine organic matter preservation could  
264 have diluted the input of terrigenous organic matter, thereby changing the relative  
265 apparent contribution.

266

#### 267 *4.4 Biomarker indicators of source and community structure*

268 Since some compounds or compound classes are associated with a particular  
269 biological source, metabolism, or physiology, molecular distributions can be informative  
270 about changes in microbial community structure. Unlike other intervals of ocean anoxia  
271 associated with mass extinction events (e.g. Xie et al., 2005; Cao et al., 2009), algal- and  
272 bacterial-derived biomarkers indicative of community structure did not vary significantly  
273 through the CIE (fig. 4). Instead, some biomarker indices that typically reflect  
274 community structure were more affected by source input at Hawsker Bottoms.

275 The regular sterane/17 $\alpha$ -hopane ratio is used as an indicator of the relative  
276 contributions of eukaryote and bacterial biomass. The regular sterane/hopane ratio was  
277 calculated using regular C<sub>27-29</sub> steranes and 17 $\alpha$  C<sub>29-33</sub> hopanes. The regular sterane/17 $\alpha$ -  
278 hopane ratio exhibited low values below -2.5 m, whereas it was more elevated (>0.5) and  
279 relatively constant in the top 10 m of the section. While this offset could be interpreted as  
280 a shift from a bacterially dominated environment in the lower part of the section to a  
281 eukaryotic environment above -3 m, it is more likely that a change in the organic matter  
282 source input is driving the regular sterane/17 $\alpha$ -hopane ratio variability. As well as  
283 containing low total steroid abundances, terrigenous organic matter can deliver hopanes  
284 derived from soil bacteria, thereby lowering the regular sterane/17 $\alpha$ -hopane ratio (Peters  
285 et al., 2005; Handley et al., 2010; Sãenz et al., 2011; French et al., 2012).

286 Similarly, small deviations are found at the bottom of the section for the C<sub>27</sub>/C<sub>27-</sub>  
287 <sub>30</sub>, C<sub>28</sub>/C<sub>27-30</sub>, and C<sub>29</sub>/C<sub>27-30</sub> sterane ratios. These ratios included regular steranes as well  
288 as diasteranes and are commonly used as indicators of the relative contribution from red  
289 algae biomass, chlorophyll-c algae, and green algae, respectively. However, they can also  
290 be affected by the delivery of C<sub>29</sub> steranes derived from land plants (Moldowan et al.,  
291 1985; Peters et al., 2005). Indeed, C<sub>29</sub> sterane was the dominant sterane in samples from  
292 the bottom of the section, where it represented nearly half of the total C<sub>27-30</sub> steranes. The  
293 C<sub>30</sub>/C<sub>27-30</sub> sterane ratio, on the other hand, which is an indicator of marine pelagophyte  
294 algae, was constant throughout the section and represented only a minor proportion of the  
295 total steranes abundance.

296 The 2 $\alpha$ -methylhopane index (2-MHI) has been used as an indicator of  
297 cyanobacterial input (Summons et al., 1999), although additional sources were later

298 reported (Rashby et al., 2007). The 3 $\beta$ -methylhopane index (3-MHI) is considered a  
299 marker for aerobic proteobacteria, including methanotrophs and acetic acid bacteria  
300 (Zundel and Rohmer, 1985; Talbot et al., 2003; Farrimond et al., 2004; Talbot and  
301 Farrimond, 2007). The 2-MHI and 3-MHI were invariant, and the 3-MHI was in the  
302 range of average Phanerozoic marine values (~1-3%) (Farrimond et al., 2004; Cao et al.,  
303 2009). Likewise, the 2-MHI also lacked elevated values. Based on elevated 2-MHI, 3-  
304 MHI, and nitrogen isotope anomalies, previous workers have reported an increased  
305 contribution of diazotrophic cyanobacteria and methanotrophic bacteria during other  
306 OAEs (e.g. Kuypers et al., 2004; Cao et al., 2009; Sepúlveda et al., 2009; Luo et al.,  
307 2011). The low and invariant contribution of these microbial groups indicates that  
308 environmental conditions suitable for their predominance did not prevail at this locality.  
309 Thus, enhanced cyanobacterial diazotrophy may not fully explain the previously reported  
310 depleted bulk organic  $\delta^{15}\text{N}$  at this location during the T-OAE (Jenkyns et al., 2001).

311

#### 312 *4.5 Indicators of redox change and depositional environment*

313 A suite of biomarkers was used to assess changes in water column stratification  
314 and redox potential, including the gammacerane index, C<sub>35</sub> homohopane index (C<sub>35</sub> HHI),  
315 pristane/phytane (Pr/Ph) ratio, and the concentration of aromatic carotenoid derivatives  
316 (fig. 5). Although some of these parameters can also be influenced by diagenesis, source  
317 input, and thermal maturity, they display patterns consistent with a shift towards more  
318 intense reducing conditions at least in the sediment porewaters and potentially in the  
319 overlying water column.

320           Although the biological sources of gammacerane are not fully known (Peters et  
321 al., 2005), it is a diagenetic product of tetrahymanol, a compound found in bacterivorous  
322 ciliates thriving at the chemocline of stratified water bodies (ten Haven et al., 1989;  
323 Sinninghe Damsté et al., 1995). Thus, the occurrence of gammacerane, expressed as the  
324 gammacerane index =  $[gammacerane / (gammacerane + 17\alpha, 21\beta C_{30} \text{ hopane})] * 100$ , has  
325 been used to infer changes in water column stratification in ancient environments.  
326 Gammacerane was detected in all of the analyzed samples but became more prominent in  
327 those deposited during the OAE, starting at the onset of thin-bedded shales.

328           Elevated abundances of gammacerane during the T-OAE may reflect the  
329 development of seasonal water column stratification, possibly due to stronger seasonality  
330 and/or deepening of the water column. In contrast, prior to the T-OAE, seasonality may  
331 have been weaker, or the water column may have been too shallow to stratify, even  
332 during warm months, due to turbulent mixing. The development of seasonal water  
333 column stratification at Hawsker Bottoms during the T-OAE would have aided the  
334 development of water column oxygen-depletion, particularly during warm and productive  
335 months. However, gammacerane enrichments alone do not necessitate water column  
336 anoxia, particularly given the association of its precursor, tetrahymanol, with suboxic  
337 waters in the modern (Wakeham et al., 2007; 2012).

338           The  $C_{35}$  HHI and Pr/Ph ratio are recorders of depositional redox conditions in  
339 sediments. The  $C_{35}$  HHI records the degree of preservation of the extended side chain of  
340  $C_{35}$  hopanes derived from intact bacteriohopanepolyols (BHPs) (Köster et al., 1997;  
341 Peters et al., 2005). Higher  $C_{35}$  HHI values are characteristic of oxygen-depleted marine  
342 depositional environments. Pristane and phytane in ancient marine rock extracts and oils



343 are largely, but not exclusively, derived from the chlorophyll phytyl side chain from  
344 photoautotrophs. Redox conditions influence the diagenetic pathway of the phytyl side  
345 chain. Reducing conditions promote the conversion of phytol to phytane, and oxic  
346 conditions promote the conversion of phytol to pristane (Didyk et al., 1978; Peters et al.,  
347 2005). The C<sub>35</sub> HHI nearly doubled in samples deposited during the OAE compared to  
348 those deposited prior to the event. Values of the Pr/Ph ratio >3 recorded at the bottom of  
349 the section are suggestive of deposition of terrigenous organic matter under oxic  
350 conditions. The Pr/Ph ratio values near or below 1 during the T-OAE, together with the  
351 elevated C<sub>35</sub> HHI, suggest intensification of reducing conditions in the sediment  
352 porewaters during deposition.

353 Biomarkers for anaerobic phototrophic green sulfur bacteria (GSB) have been  
354 used to argue for the development of PZE during the T-OAE (Schouten et al., 2000;  
355 Pancost et al., 2004; Bowden et al., 2006) and other OAEs (e.g. Cao et al., 2009) based  
356 on the physiological requirement of co-occurring reduced sulfur species and light. We  
357 detected 2,3,6-aryl isoprenoids, isorenieratane, and chlorobactane in all samples. Unlike  
358 previous studies of the T-OAE or any Phanerozoic organic geochemical study of marine  
359 samples, trace concentrations of okenane were also identified by GC-MRM-MS in  
360 samples above -3 m, whereas it was below detection limit in samples from the lowest 2  
361 meters of the section. Okenone, a photosynthetic pigment belonging to the PSB family  
362 Chromatiaceae, is the only known precursor of okenane (Brocks and Schaeffer, 2008).  
363 All compounds were compared with an authentic carotenoid standard and an extract from  
364 the Barney Creek Formation (BCF; fig. 6; Brocks et al., 2005). Normalizations of the C<sub>40</sub>

365 aromatic carotenoid derivatives against the mass of TOC and TLE reveal a similar pattern  
366 of elevated concentrations during the anoxic event compared to the pre-event baseline.

367 In total, all of the organic geochemical redox indicators point towards a shift  
368 towards more reducing conditions broadly corresponding with the initiation of the  
369 negative CIE. However, sedimentological features, such as starved wave and combined  
370 flow ripples, indicate that this area was an energetic, shallow inner shelf environment on  
371 the order of tens of meters and probably no deeper than 50 m, where enough oxygen was  
372 present in the water column on some timescale to sustain nektonic fauna, including  
373 ammonites, and allow for bioturbation at the sediment-water interface through the OAE  
374 (Wignall et al., 2005; Powell, 2010; Ghadeer and Macquaker, 2011). We explore  
375 different scenarios to reconcile these apparent opposing lines of evidence.

376 First, the geochemical and sedimentological signals recorded in the rock record  
377 are a composite of many processes occurring on different timescales. In the modern  
378 ocean, highly productive coastal and continental margin sediments and the overlying  
379 water column oscillate between oxic and anoxic conditions over different timescales (e.g.  
380 Burdige, 2007). Enhanced productivity and export of organic matter, which are important  
381 features of Mesozoic OAEs (e.g. Erba, 2004; Jenkyns, 2010), would have increased the  
382 oxygen demand in the water column and sediment porewaters during productive months.  
383 During the T-OAE, anoxic conditions may have been restricted to the sediment  
384 porewaters during seasons of low productivity, allowing bioturbation to occur when  
385 bottom waters were better oxygenated. Conversely, oxygen-deficient waters may have  
386 expanded seasonally to the water column during intervals of high productivity and  
387 enhanced stratification, as implied by the gammacerane index.

388           Second, the molecular, paleontological, and sedimentary indicators of redox  
389 chemistry apply to different parts of the depositional environment, diagenetic pathways,  
390 and have different sensitivities along the redox spectrum. With the exception of the GSB  
391 and PSB carotenoid markers, the geochemical parameters reported here do not require  
392 strict anoxia or euxinia in the water column. The gammacerane index pattern supports the  
393 development of seasonal stratification during the OAE, which would have promoted  
394 oxygen depletion of the water column. However, the possibility remains that even during  
395 intervals of high productivity and stratification, water column oxygen concentrations at  
396 this location were depleted but high enough to sustain organisms with physiological  
397 oxygen requirements, thereby explaining the fossil and sedimentary evidence.  
398 Additionally, the Pr/Ph ratio and C<sub>35</sub> HHI pertain primarily to sedimentary redox  
399 conditions opposed to water column redox structure. Therefore, the occurrence of intact  
400 aromatic carotenoid derivatives merits further discussion to assess water column redox  
401 chemistry.

402           To date, okenane has only been reported in Paleoproterozoic rock extracts and  
403 lacustrine Cenozoic extracts (Brocks et al., 2005; Zhang et al., 2011). Given the  
404 atmospheric  $pO_2$  during the Mesozoic was near present atmospheric levels (Berner,  
405 2006), its detection in marine samples of this age requires careful interpretation. The PSB  
406 family Chromatiaceae blooms in a range of anoxic environments with light and reduced  
407 sulfur species, including stratified lakes, fjords, coastal lagoons, estuaries, and coastal  
408 microbial mats, but not all Chromatiaceae produce okenone (Brocks and Schaeffer, 2008  
409 and references therein). Okenone-producing planktonic Chromatiaceae dwell in water  
410 columns where the chemocline is above 25 m and in 75% of the reported cases less than

411 12 m (Brocks and Schaeffer, 2008). Notably, all of the modern chemocline depth  
412 observations for okenone production are based on stratified lake systems. Thus, the lack  
413 of okenone in modern marine sulfidic environments presents a “no analogue problem” for  
414 ancient marine samples containing okenane that were deposited under atmospheric  $pO_2$   
415 close to modern levels.

416         Transient free sulfide has been reported in the water column of intense upwelling  
417 zones, including the Arabian Sea, Namibian coast, and the Peruvian coast (e.g Dugdale et  
418 al., 1977; Brüchert et al., 2003; Naqvi et al., 2006; Schunck et al., 2013). However, these  
419 episodes are typically short lived. In contrast, sulfidic waters persist in some restricted  
420 marine basins and fjords, including the Black Sea, Cariaco Basin, Saanich Inlet, and the  
421 Framvaren and Effingham Fjords. However, these two types of marine environments  
422 (non-restricted, transiently sulfidic and restricted, permanently sulfidic) fail to represent  
423 suitable modern analogues for Hawsker Bottoms on several counts. Isoorenieratene has  
424 been measured in the water column and sediments of some restricted marine basins,  
425 particularly fjords and the Black Sea (e.g. Sinninghe Damsté and Schouten, 2006), but  
426 GSB carotenoids have not been detected in transiently sulfidic upwelling systems.  
427 Furthermore, okenone has not been reported in the water column or sediments of any  
428 modern marine transiently or permanently sulfidic environment, with the exception of the  
429 upper sediments of Kyllaren fjord, a small, highly restricted basin (Smittenberg et al.,  
430 2004; Sinninghe Damsté and Schouten, 2006). Like okenone, modern planktonic marine  
431 occurrences of chlorobactene are also limited to semi-enclosed water masses that are not  
432 representative of fully marine conditions (e.g. Naeher et al. 2012). Interestingly, multiple  
433 emerging lines of evidence suggest the occurrence of a “cryptic sulfur cycle” in some

434 OMZs, with a potential role for photosynthetic sulfide oxidation (Canfield et al., 2010;  
435 Stewart et al., 2012). However, the presence of GSB and/or PSB and their respective  
436 carotenoids have yet to be reported in modern OMZs.

437         Furthermore, the physical oceanographic processes determining the degree of  
438 vertical mixing, hence stratification and redox gradient stability, are markedly different  
439 between inner shelf environments and sulfidic, silled basins, which are highly restricted  
440 and in many classic modern examples, are an order of magnitude or more deeper than  
441 estimated paleodepths of Hawsker Bottoms. Although the water column at Hawsker  
442 Bottoms became deeper with the sea level transgression across the T-OAE, the  
443 depositional environment remained relatively shallow because of its location on a gently  
444 sloping shelf (e.g. Macquaker et al., 2010). Consequently, turbulent mixing at the surface  
445 and bottom boundary layers would have prevented a stable sulfidic chemocline from  
446 developing. On the other hand, considering the limited occurrence of planktonically  
447 produced okenone in modern lakes, a planktonic source of okenone at Hawsker Bottoms  
448 would imply that, rather than an inner shelf environment, Hawsker Bottoms was a highly  
449 restricted coastal basin not reflective of fully marine conditions.

450         Alternatively, we argue that okenane at Hawsker Bottoms was likely derived from  
451 benthic microbial mats based on the lack of modern analogues of okenone-production in  
452 marine sulfidic environments, the dynamics of inner shelf physical mixing, and building  
453 evidence of okenone-producing, mat-dwelling Chromatiaceae (e.g. Caumette et al., 1991;  
454 Airs et al., 2001; Caumette et al., 2004; Meyer et al., 2011). Furthermore, planktonic  
455 Chlorobiaceae are not the exclusive source of isorenieratene and chlorobactene. Previous  
456 work has documented additional non-planktonic GSB sources of isorenieratene and

457 chlorobactene, including microbial mats (e.g. Wahlund et al., 1991; Brocks and  
458 Summons, 2003; Beatty et al., 2005; Bühring et al., 2011). Although a mixed planktonic  
459 and mat origin of the carotenoids cannot be ruled out, it is more likely that the GSB and  
460 PSB carotenoids detected in Hawsker Bottoms samples share a source. Previous studies  
461 of sedimentary structures in the Toarcian shales of Yorkshire have attributed wavy  
462 laminations to microbial mats (O'Brien, 1990), thereby further supporting a sedimentary  
463 origin of GSB and PSB carotenoid derivatives detected in Hawsker Bottoms samples.  
464 Similar wavy laminated fabrics have been reported in coeval shales in northern European  
465 T-OAE sections (Trabucho-Alexandre et al., 2012). Unfortunately, a sedimentary source  
466 of the GSB and PSB carotenoid derivatives offers little information about water column  
467 redox chemistry. However, this interpretation does not preclude the development of a  
468 suboxic, anoxic, or euxinic water column in this region on some timescale during the T-  
469 OAE. Instead, additional inorganic geochemical data is required to better assess the water  
470 column redox conditions and degree of basin restriction (Algeo and Tribovillard, 2009).

471

#### 472 *4.6 Compound specific stable carbon isotopic data*

473 A limited number of compound specific  $\delta^{13}\text{C}$  records of the T-OAE are currently  
474 available in the literature. Here, we report the first long-chain *n*-alkane  $\delta^{13}\text{C}$  records of  
475 the T-OAE. Compound specific  $\delta^{13}\text{C}$  analyses of marine- and terrestrial-derived lipids  
476 reveal a shift towards lighter  $\delta^{13}\text{C}$  values (fig. 7). Short-chain *n*-alkanes, as well as  
477 pristane and phytane are typically used as marine indicators, whereas long-chain *n*-  
478 alkanes primarily reflect terrigenous sources. The *n*-C<sub>17</sub>, *n*-C<sub>18</sub>, and *n*-C<sub>19</sub> alkanes  
479 displayed a negative excursion of ~2–3‰, which is consistent with the ~2–4‰ negative

480 excursions documented in the partial  $n$ -C<sub>16-20</sub> alkane records from the Toarcian  
481 Posidonienschiefer in southwest Germany (Schouten et al., 2000). Pristane and phytane  
482 encode a muted excursion ( $\sim 1.5$ – $2\%$ ) compared to short-chain alkane records, and they  
483 also have smaller CIE magnitudes compared to the pristane and phytane isotopic records  
484 from the Toarcian Paris Basin and the Posidonienschiefer ( $\sim 3$ – $4\%$ ) (Schouten et al.,  
485 2000; van Breugel et al., 2006). On the other hand, long-chain  $n$ -alkanes ( $n$ -C<sub>27</sub>,  $n$ -C<sub>28</sub>,  
486 and  $n$ -C<sub>29</sub>), which are primarily but not exclusively derived from epicuticular waxes of  
487 vascular plants (Eglinton and Hamilton, 1967), display the largest compound specific  
488 negative CIE ( $\sim 4$ – $5\%$ ). The molecular isotopic records appear to register the initiation of  
489 the negative CIE earlier than in the bulk organic record, and within the CIE, the  
490 compound-specific  $\delta^{13}\text{C}$  values remain fairly stable while the bulk curve becomes  
491 gradually depleted. However, these features could be due to sampling resolution  
492 differences. Higher resolution molecular isotopic records are required to better address  
493 the timing and structure of the isotopic excursion recorded in different carbon reservoirs.

494 The absolute magnitude of the bulk organic CIE ( $\sim 5$ – $7\%$ ) is larger than the CIEs  
495 recorded in the molecular records from Yorkshire (this study;  $\sim 1.5$ – $5\%$ ), the Paris Basin  
496 ( $\sim 3\%$ ; van Breugel et al., 2006), and the Posidonienschiefer ( $\sim 2$ – $4\%$ ; Schouten et al.,  
497 2000). Identifying the reason behind the CIE magnitude offsets is critical for placing  
498 bounds on the magnitude of isotopically light carbon added into the system. Bulk organic  
499 matter is comprised of an array of molecularly and isotopically heterogeneous  
500 constituents. In addition to environmental perturbations, organic matter source mixing  
501 can contribute to bulk organic  $\delta^{13}\text{C}$  excursions (e.g. Pancost et al., 1999). The comparison  
502 of short- and long-chain  $n$ -alkane isotopic compositions demonstrates that, unlike the

503 modern, terrigenous organic matter is isotopically heavier than marine organic matter  
504 during the Toarcian (fig. 7), which is consistent with previous Toarcian studies (Vetö et  
505 al., 1997; Schouten et al., 2000). Multiple lines of evidence presented in section 4.3  
506 highlight a significant transition in the terrigenous organic matter input at Hawsker  
507 Bottoms. Indeed, the bottom 2 meters of the study interval are dominated by terrigenous  
508 organic matter and are isotopically heavier than the overlying interval that is dominated  
509 by marine organic matter. Therefore, an undetermined component of the bulk organic  
510 CIE magnitude may be attributed to source mixing effects.

511         Additional factors could also contribute to the difference in magnitudes between  
512 bulk and molecular CIEs. For instance, it is possible that the full CIE was not captured in  
513 the molecular isotopic records due to a lower sampling resolution compared to the bulk  
514 organic  $\delta^{13}\text{C}$  records. Alternatively, water availability can modulate the magnitude of the  
515 CIE recorded in vascular leaf waxes, as has been discussed for the Paleocene Eocene  
516 Thermal Maximum (PETM; e.g. Schouten et al., 2007; Smith et al., 2007), but unlike the  
517 PETM, the ratio of angiosperms and conifers would not account for the *n*-alkane and bulk  
518 organic CIE magnitude offset because the rise of angiosperms postdates the Early  
519 Jurassic (e.g. Heimhofer et al., 2005). Additionally, thermal maturation could influence  
520 the  $\delta^{13}\text{C}$  of individual compounds, which become isotopically heavier with increasing  
521 thermal maturity (Clayton, 1991; Clayton and Bjorøy, 1994; Tang et al., 2005).

522         Nevertheless, while multiple mechanisms may account for the difference between  
523 molecular and bulk organic CIE magnitudes, it is significant that a negative CIE is  
524 recorded in both marine- and terrestrial-derived lipids, albeit to different degrees. The  
525 parallel isotopic change in marine and terrestrial carbon pools recorded at Hawsker



526 Bottoms further supports previous studies suggesting that the T-OAE was a global carbon  
527 cycle perturbation where isotopically light carbon entered the atmospheric, terrigenous,  
528 and marine carbon reservoirs (Hesselbo et al., 2000; 2007; Al-Suwaidi et al., 2010;  
529 Caruthers et al., 2011; Gröcke et al., 2011). Multiple sources of isotopically light carbon  
530 have been proposed, including methane hydrate dissociation, regional upwelling of  
531 isotopically light waters in stratified epicontinental seas, thermogenic release of methane  
532 from organic-rich strata in contact with dykes, biomass burning, or a combination of  
533 these mechanisms (Hesselbo et al., 2000; Schouten et al., 2000; McElwain et al., 2005;  
534 van de Schootbrugge et al., 2005; Finkelstein et al., 2006).

535         Although our study does not provide evidence in support of a specific forcing  
536 mechanism, it allows us to narrow down potential mechanisms. A deep-water source of  
537 isotopically light carbon is unlikely because of the CIE observed in land plant  
538 biomarkers. The lack of evidence for bacterial methanotrophy in our section suggests that  
539 methane hydrate dissociation did not supply appreciable methane to the sampling  
540 locality. The organic matter source transition complicates the interpretation of PAH  
541 abundances as tracers of biomass burning, so a different sampling locality without an  
542 organic matter source transition should be studied to test the biomass burning mechanism  
543 using PAHs. A cascade of mechanisms rather than a single mechanism likely initiated the  
544 T-OAE. However, our results indicate that the influence of source mixing on the bulk  
545 organic  $\delta^{13}\text{C}$  has been previously underestimated and could have potentially affected  
546 other bulk isotopic systematics such as nitrogen. Therefore, previous estimates regarding  
547 the magnitude of this global perturbation of the carbon cycle should be revisited.

548

## 549 **5. Conclusions**

550 We use a multiproxy approach based on bulk geochemistry, lipid biomarkers, and  
551 compound-specific stable isotopes to elucidate environmental and ecological changes  
552 associated with the T-OAE at Hawsker Bottoms in Yorkshire, England. Molecular  
553 indicators and Rock-Eval results suggest that thermal maturity is uniformly in the early  
554 oil generation window throughout the sampling interval. The HI data, organic  
555 petrography, PAH distribution, and tricyclic terpane ratios indicate a transition in the  
556 relative input of terrigenous vs. marine organic matter across a lithological transition. The  
557 shift to lower relative abundance of terrigenous organic matter was likely a result of sea  
558 level related effects such as coastal proximity, changes in marine organic matter  
559 preservation, and/or dilution effects from increased marine productivity.

560 Organic geochemical redox and depositional environment indicators point  
561 towards an overall shift towards more reducing conditions in sediment porewaters and the  
562 development of seasonal stratification during the OAE. Previous sedimentological  
563 observations require that the water column was not completely anoxic throughout the  
564 entire T-OAE, which may seem contradictory at first to the detection of GSB and PSB  
565 carotenoids. However, here we present the first occurrence of okenane, a carotenoid  
566 marker of PSB, in marine samples younger than the Paleoproterozoic (1.64 Ga). This  
567 unexpected finding challenges the interpretation of GSB and PSB carotenoids as markers  
568 of PZE in the context of Hawsker Bottoms due to inner shelf vertical mixing, the lack of  
569 modern analogues of okenone-production in marine sulfidic environments, and the  
570 emerging evidence of okenone-producing mat-dwelling Chromatiaceae. Therefore, in  
571 combination with previous reports of microbial wavy lamination in Toarcian shales of

572 Yorkshire and coeval shales in northern Europe, we argue that okenane, and potentially  
573 chlorobactane and isorenieratane, was most likely mat-derived at Hawsker Bottoms.

574 The compound-specific  $\delta^{13}\text{C}$  records of short-chain *n*-alkanes, acyclic  
575 isoprenoids, and long-chain *n*-alkanes support a carbon cycle perturbation that affected  
576 both the atmospheric and marine systems, which precludes the recycling of isotopically  
577 light  $\text{CO}_2$  from anoxic waters as the sole mechanism responsible for the T-OAE negative  
578 CIE. Notably, compound specific  $\delta^{13}\text{C}$  records of the T-OAE, including the new data  
579 presented here from Yorkshire and previous molecular data from the Paris Basin and the  
580 Posidonienschiefer, encode negative CIEs that are smaller in magnitude compared to bulk  
581 organic  $\delta^{13}\text{C}$  records. Many mechanisms could contribute to this observation, particularly  
582 variable mixing of terrigenous and marine organic matter, which is supported by the  
583 multiple lines of evidence for a transition in organic matter source. Identifying the  
584 mechanisms behind the CIE magnitude offsets is important for estimating the magnitude  
585 of isotopically light carbon injected into the surface carbon reservoirs.

586

#### 587 Acknowledgements

588 We thank Alison Cohen and Emma Grosjean for their contributions to the early  
589 stages of this study, Lorraine Eglinton for petrographic analysis, Carolyn Colonero for  
590 laboratory assistance, and three anonymous reviewers for valuable comments that  
591 improved this work. Funding support for work at MIT was provided by grants from the  
592 NASA Astrobiology Institute and the NASA Exobiology Program to RES and an NSF  
593 graduate fellowship to KLF. This project was partly funded by a NSERC Discovery

594 Grant (# 288321) and NERC Standard Grant (NE/H021868/1) to DRG. JTA is funded by  
595 the NERC Standard Grant (NE/H021868/1) to DRG.

596

597 Figure Captions:

598 **Fig. 1. Rock-Eval Analysis.** A) Total organic carbon (TOC; %) (Hesselbo et al., 2000);  
599 B) Hydrogen index (HI; mg HC/g TOC); C) Production index (PI); D)  $T_{max}$  (°C).

600

601 **Fig. 2. Molecular Indicators of Thermal Maturity.** A) The  $C_{31}$  hopane 22S/(22S+22R)  
602 ratio; B)  $C_{30}$  hopane  $\beta\alpha/(\beta\alpha+\alpha\beta)$  ratio; C)  $C_{29}$  sterane  $\alpha\alpha\alpha$  20S/(20S+20R) ratio; D)  
603 Ts/(Ts+Tm) ratio; E) diasteranes/steranes ratio. Note the lack of variation in A, B and C  
604 across the section compared to the minor variations exhibited by D and E due to changes  
605 in source input and/or lithology.

606

607 **Fig 3. Terrigenous Organic Matter Indicators.** A) Ratios of  $C_{19}/C_{23}$  and  $C_{20}/C_{23}$   
608 tricyclic terpanes; B) total concentration of PAHs normalized by TOC and TLE; C)  
609 concentration of retene normalized by TOC and TLE; D) measured contribution of  
610 terrigenous organic matter (OM) by petrographic analysis; E) calculated percentage of  
611 terrigenous organic matter ( $f_{Terr\ OM}$ ) based on linear regression ( $f_{Terr\ OM} (\%) = -0.279 * HI$   
612  $+ 136$ ;  $R^2=0.90$ ) of petrographic measurements of terrigenous organic matter (Fig. 3D)  
613 and HI (Fig. 1B).

614

615 **Fig. 4. Source and Community Indicators.** A) The ratio of regular steranes/17 $\alpha$ -  
616 hopanes; B)  $C_{27}/C_{27-30}$  steranes; C)  $C_{28}/C_{27-30}$  steranes; D)  $C_{29}/C_{27-30}$  steranes; E) 2 $\alpha$ -  
617 methylhopane and 3 $\beta$ -methylhopane indices.

618

619 **Fig. 5. Redox and Depositional Environmental Indicators.** A) Gammacerane index; B)  
620  $C_{35}$  homohopane index ( $C_{35}HHI$ ); C) pristane/phytane (Pr/Ph) ratio; D) concentration of  
621 isorenieratane; E) concentration of chlorobactane; F) concentration of okenane. The  
622 concentrations of  $C_{40}$  carotenoids are semi-quantitative and were normalized against TOC  
623 and TLE.

624

625 **Fig. 6 Gas chromatography - metastable reaction monitoring - mass spectrometry**  
626 **(GC-MRM-MS) chromatogram for the identification of aromatic carotenoid**  
627 **derivatives.** MRM chromatograms displaying the 554→134 transition characteristic for  
628 chlorobactane and okenane in an authentic standard of combined  $C_{40}$  carotenoids (A) and  
629 in sample ENR004 at 5.98 m (C). Plots B and D are MRM chromatograms displaying the  
630 546→134 MRM transition characteristic of isorenieratane, renieratane, and  
631 renierapurpurane in an authentic standard of combined  $C_{40}$  carotenoid (B) and in sample  
632 ENR004 (D). Compound abbreviations were used for labels: chlorobactane (Ch);  
633 okenane (Ok); isorenieratane (Iso); renieratane (Ren); renierapurpurane (Rpurp).

634

635 **Fig. 7 Carbon Isotopic records.** A) Previously reported  $\delta^{13}\text{C}_{\text{org}}$  from Hawsker Bottoms  
636 (Hesselbo et al., 2000; Kemp et al., 2005); B)  $\delta^{13}\text{C}$  of n-C<sub>17-19</sub> short-chain n-alkanes; C)  
637  $\delta^{13}\text{C}$  of pristane and phytane; D)  $\delta^{13}\text{C}$  of n-C<sub>27-29</sub> long-chain n-alkanes. Note the different  
638 x-axis scales.  
639

640 References

641

- 642 Airs, R.L., Atkinson, J.E., Keely, B.J., 2001. Development and application of a high  
643 resolution liquid chromatographic method for the analysis of complex pigment  
644 distributions. *J. Chromatogr. A* 917, 167–177.
- 645 Algeo, T. J., Tribovillard, N., 2009. Environmental analysis of paleoceanographic  
646 systems based on molybdenum-uranium covariation. *Chem. Geol.* 268, 211–225.
- 647 Al-Suwaidi, A.H., Angelozzi, G.N., Baudin, F., Damborenea, S.E., Hesselbo, S.P.,  
648 Jenkyns, H.C., Mancenido, M.O., Riccardi, A.C., 2010. First record of the Early  
649 Toarcian Oceanic Anoxic Event from the Southern Hemisphere, Neuquén Basin,  
650 Argentina. *J. Geol. Soc. (London)* 167, 633–636.
- 651 Arinobu, T., Ishiwatari, R., Kaiho, K., Lamolda, M.A., 1999. Spike of pyrosynthetic  
652 polycyclic aromatic hydrocarbons associated with an abrupt decrease in  $\delta^{13}\text{C}$  of a  
653 terrestrial biomarker at the Cretaceous-Tertiary boundary at Caravaca, Spain.  
654 *Geology* 27, 723–726.
- 655 Bambach, R.K., 2006. Phanerozoic biodiversity mass extinctions. *Annu. Rev. Earth*  
656 *Planet. Sci.* 34, 127–155.
- 657 Beatty, J., Overmann, J., Lince, M., Manske, A., Lang, A., Blankenship, R., Van Dover,  
658 C., Martinson, T., Plumley, F., 2005. An obligately photosynthetic bacterial anaerobe  
659 from a deep-sea hydrothermal vent. *Proc. Natl. Acad. Sci. U.S.A* 102, 9306–9310.
- 660 Bennett, B., Olsen, S., 2007. The influence of source depositional conditions on the  
661 hydrocarbon and nitrogen compounds in petroleum from central Montana, USA. *Org.*  
662 *Geochem.* 38, 935–956.
- 663 Berner, R., 2006. GEOCARBSULF: A combined model for Phanerozoic atmospheric  $\text{O}_2$   
664 and  $\text{CO}_2$ . *Geochim. Cosmochim. Acta* 70, 5653–5664.
- 665 Bowden, S.A., Farrimond, P., Snape, C.E., Love, G.D., 2006. Compositional differences  
666 in biomarker constituents of the hydrocarbon, resin, asphaltene and kerogen  
667 fractions: An example from the Jet Rock (Yorkshire, UK). *Org. Geochem.* 37, 369–  
668 383.
- 669 Bradshaw, M J, J C W Cope, D W Cripps, D T Donovan, M K Howarth, P F Rawson, I  
670 M West, and W A Wimbledon. 1992. “Jurassic.” *Geol. Soc., London, Memoirs* 13,  
671 107–129.
- 672 Brocks, J., Love, G., Summons, R., Knoll, A., Logan, G., Bowden, S., 2005. Biomarker  
673 evidence for green and purple sulphur bacteria in a stratified Palaeoproterozoic sea.  
674 *Nature* 437, 866–870.
- 675 Brocks, J., Schaeffer, P., 2008. Okenane, a biomarker for purple sulfur bacteria  
676 (Chromatiaceae), and other new carotenoid derivatives from the 1640 Ma Barney  
677 Creek Formation. *Geochim. Cosmochim. Acta* 72, 1396–1414.
- 678 Brocks, J.J., Summons, R.E., 2003. Sedimentary hydrocarbons, biomarkers for early life.  
679 In: *Treatise on Geochemistry*, (Elsevier-Pergamon, Oxford). Chpt. 8.03, pp. 63–115.
- 680 Brüchert, V., Jørgensen, B.B., Neumann, K., Riechmann, D., Schlösser, M., Schulz, H.,  
681 2003. Regulation of bacterial sulfate reduction and hydrogen sulfide fluxes in the  
682 central Namibian coastal upwelling zone. *Geochim. Cosmochim. Acta* 67, 4505–  
683 4518.
- 684 Burdige, D., 2007. Preservation of organic matter in marine sediments: controls,  
685 mechanisms, and an imbalance in sediment organic carbon budgets? *Chem. Rev.*

686 107, 467–485.

687 Böhling, S., Sievert, S., Jonkers, H., Ertefai, T., Elshahed, M., Krumholz, L., Hinrichs, K.  
688 -U., 2011. Insights into chemotaxonomic composition and carbon cycling of  
689 phototrophic communities in an artesian sulfur-rich spring (Zodletone, Oklahoma,  
690 USA), a possible analog for ancient microbial mat systems. *Geobiol.* 9, 166–179.

691 Canfield, D.E., Stewart, F.J., Thamdrup, B., De Brabandere, L., Dalsgaard, T., Delong,  
692 E.F., Revsbech, N.P., Ulloa, O., 2010. A Cryptic Sulfur Cycle in Oxygen-Minimum-  
693 Zone Waters off the Chilean Coast. *Science* 330, 1375–1378.

694 Cao, C., Love, G.D., Hays, L., Wang, W., Shen, S., Summons, R.E., 2009.  
695 Biogeochemical evidence for euxinic oceans and ecological disturbance presaging  
696 the end-Permian mass extinction event. *Earth Planet. Sci. Lett.* 281, 188–201.

697 Caruthers, A.H., Gröcke, D.R., Smith, P.L., 2011. The significance of an Early Jurassic  
698 (Toarcian) carbon-isotope excursion in Haida Gwaii (Queen Charlotte Islands),  
699 British Columbia, Canada. *Earth Planet. Sci. Lett.* 307, 19–26.

700 Caumette, P., Baulaigue, R., Matheron, R., 1991. *Thiocapsa halophila* sp. nov., a new  
701 halophilic phototrophic purple sulfur bacterium. *Arch. Microbiol.* 155, 170–176.

702 Caumette, P., Guyoneaud, R., Imhoff, J., Süling, J., Gorlenko, V., 2004. *Thiocapsa*  
703 *marina* sp. nov., a novel, okenone-containing, purple sulfur bacterium isolated from  
704 brackish coastal and marine environments. *Int. J. Syst. Evol. Microbiol.* 54, 1031–  
705 1036.

706 Clayton, C., 1991. Effect of maturity on carbon isotope ratios of oils and condensates.  
707 *Org. Geochem.* 17, 887–899.

708 Clayton, C., Bjorøy, M., 1994. Effect of maturity on  $^{13}\text{C}/^{12}\text{C}$  ratios of individual  
709 compounds in North Sea oils. *Org. Geochem.* 21, 737–750.

710 Cohen, A.S., Coe, A.L., Harding, S.M., Schwark, L., 2004. Osmium isotope evidence for  
711 the regulation of atmospheric  $\text{CO}_2$  by continental weathering. *Geology* 32, 157–160.

712 Courtillot, V.E., Renne, P.R., 2003. On the ages of flood basalt events. *C. R. Geoscience*  
713 335, 113–140.

714 Dahl, J., Moldowan, J., M., Sundararaman, P., 1993. Relationship of biomarker  
715 distribution to depositional environment: Phosphoria Formation, Montana, USA.  
716 *Org. Geochem.* 20, 1001–1017.

717 Didyk, B., Simoneit, B., Brassell, S., Eglinton, G., 1978. Organic geochemical indicators  
718 of palaeoenvironmental conditions of sedimentation. *Nature* 272, 216–222.

719 Dugdale, R., Goering, J., Barber, R., Smith, R., Packard, T., 1977. Denitrification and  
720 hydrogen sulfide in the Peru upwelling region during 1976. *Deep-Sea Res.* 24, 601–  
721 608.

722 Eglinton, G., Hamilton, R., 1967. Leaf epicuticular waxes. *Science.* 156, 1322–1335.

723 Ellis, L., Singh, R.K., Alexander, R., Kagi, R.I., 1996. Formation of isohexyl  
724 alkylaromatic hydrocarbons from aromatization-rearrangement of terpenoids in the  
725 sedimentary environment: A new class of biomarker. *Geochim. Cosmochim. Acta*  
726 60, 4747–4763.

727 Erba, E., 2004. Calcareous nannofossils and Mesozoic oceanic anoxic events. *Mar.*  
728 *Micropaleontol.* 52, 85–106.

729 Farrimond, P., Eglinton, G., Brassell, S., Jenkyns, H., 1989. Toarcian anoxic event in  
730 Europe: an organic geochemical study. *Mar. Petrol. Geol.* 6, 136–147.

731 Farrimond, P., Stoddart, D., Jenkyns, H., 1994. An Organic Geochemical Profile of the

732 Toarcian Anoxic Event in Northern Italy. *Chem. Geol.* 111, 17–33.

733 Farrimond, P., Talbot, H.M., Watson, D.F., Schulz, L.K., Wilhelms, A., 2004.

734 Methylhopanoids: Molecular indicators of ancient bacteria and a petroleum

735 correlation tool. *Geochim. Cosmochim. Acta* 68, 3873–3882.

736 Finkelstein, D.B., Pratt, L.M., Brassell, S.C., 2006. Can biomass burning produce a

737 globally significant carbon-isotope excursion in the sedimentary record? *Earth*

738 *Planet. Sci. Lett.* 250, 501–510.

739 Finkelstein, D.B., Pratt, L.M., Curtin, T.M., Brassell, S.C., 2005. Wildfires and seasonal

740 aridity recorded in Late Cretaceous strata from south-eastern Arizona, USA.

741 *Sedimentology* 52, 587–599.

742 French, K.L., Tosca, N.J., Cao, C., Summons, R.E., 2012. Diagenetic and detrital origin

743 of moretane anomalies through the Permian–Triassic boundary. *Geochim.*

744 *Cosmochim. Acta* 84, 104–125.

745 George, S.C., 1992. Effect of igneous intrusion on the organic geochemistry of a siltstone

746 and an oil shale horizon in the Midland Valley of Scotland. *Org. Geochem.* 18, 705–

747 723.

748 Ghadeer, S.G., Macquaker, J.H.S., 2011. Sediment transport processes in an ancient mud-

749 dominated succession: a comparison of processes operating in marine offshore

750 settings and anoxic basinal environments. *J. Geol. Soc. (London)* 168, 1121–1132.

751 Grice, K., Backhouse, J., Alexander, R., Marshall, N., Logan, G.A., 2005. Correlating

752 terrestrial signatures from biomarker distributions,  $\delta^{13}\text{C}$ , and palynology in fluvio-

753 deltaic deposits from NW Australia (Triassic–Jurassic). *Org. Geochem.* 36, 1347–

754 1358.

755 Grice, K., Nabbefeld, B., Maslen, E., 2007. Source and significance of selected

756 polycyclic aromatic hydrocarbons in sediments (Hovea-3 well, Perth Basin, Western

757 Australia) spanning the Permian-Triassic boundary. *Org. Geochem.* 38, 1795–1803.

758 Gröcke, D., Hori, R., Trabucho-Alexandre, J., Kemp, D., Schwark, L., 2011. An open

759 marine record of the Toarcian oceanic event. *Solid Earth* 2, 245–257.

760 Handley, L., Talbot, H.M., Cooke, M.P., Anderson, K.E., Wagner, T., 2010.

761 Bacteriohopanepolyols as tracers for continental and marine organic matter supply

762 and phases of enhanced nitrogen cycling on the late Quaternary Congo deep sea fan.

763 *Org. Geochem.* 41, 910–914.

764 Heimhofer, U., P. A. Hochuli, S. Burla, J. M. L. Dinis, and H. Weissert., 2005. Timing of

765 Early Cretaceous angiosperm diversification and possible links to major

766 paleoenvironmental change. *Geology* 33, 141–144.

767 Hesselbo, S., 2008. Sequence stratigraphy and inferred relative sea-level change from the

768 onshore British Jurassic. *P. Geologist Assoc.* 119, 19–34.

769 Hesselbo, S., Jenkyns, H., 1995. A comparison of the Hettangian to Bajocian successions

770 of Dorset and Yorkshire, in: Taylor, P. (Ed.), *Field Geology of the British Jurassic.*

771 *Geological Society of London*, pp. 105–150.

772 Hesselbo, S.P., Gröcke, D.R., Jenkyns, H.C., Bjerrum, C.J., Farrimond, P., Morgans Bell,

773 H.S., Green, O.R., 2000. Massive dissociation of gas hydrate during a Jurassic

774 oceanic anoxic event. *Nature* 406, 392–395.

775 Hesselbo, S.P., Jenkyns, H.C., Duarte, L.V., Oliveira, L.C.V., 2007. Carbon-isotope

776 record of the Early Jurassic (Toarcian) Oceanic Anoxic Event from fossil wood and

777 marine carbonate (Lusitanian Basin, Portugal). *Earth Planet. Sci. Lett.* 253, 455–470.



778 Hites, R.A., Laflamme, R.E., Farrington, J.W., 1977. Sedimentary Polycyclic Aromatic  
779 Hydrocarbons: The Historical Record. *Science* 198, 829–831.

780 Howarth, M., 1992. The ammonite family Hildoceratidae in the Lower Jurassic of  
781 Britain. *Palaeontogr. Soc. Monogr.* 145, 1–106.

782 Jenkyns, H., 1988. The early Toarcian (Jurassic) anoxic event: stratigraphic, sedimentary,  
783 and geochemical evidence. *Am. J. Sci.* 288, 101–151.

784 Jenkyns, H., Gröcke, D., Hesselbo, S., 2001. Nitrogen isotope evidence for water mass  
785 denitrification during the early Toarcian (Jurassic) oceanic anoxic event.  
786 *Paleoceanography* 16, 593–603.

787 Jenkyns, H.C., 1980. Cretaceous anoxic events: from continents to oceans. *J. Geol. Soc.*  
788 (London) 137, 171–188.

789 Jenkyns, H.C., 2010. Geochemistry of oceanic anoxic events. *Geochem. Geophys.*  
790 *Geosyst.* 11, Q03004.

791 Jiang, C., Alexander, R., Kagi, R.I., Murray, A.P., 1998. Polycyclic aromatic  
792 hydrocarbons in ancient sediments and their relationships to palaeoclimate. *Org.*  
793 *Geochem.* 29, 1721–1735.

794 Jiang, C., Alexander, R., Kagi, R.I., Murray, A.P., 2000. Origin of perylene in ancient  
795 sediments and its geological significance. *Org. Geochem.* 31, 1545–1559.

796 Kawka, O.E., Simoneit, B.R.T., 1990. Polycyclic aromatic hydrocarbons in hydrothermal  
797 petroleum from the Guaymas Basin spreading center. *Appl. Geochem.* 5, 17–27.

798 Kemp, D.B., Coe, A.L., Cohen, A.S., Schwark, L., 2005. Astronomical pacing of  
799 methane release in the Early Jurassic period. *Nature* 437, 396–399.

800 Kemp, D.B., Coe, A.L., Cohen, A.S., Weedon, G.P., 2011. Astronomical forcing and  
801 chronology of the early Toarcian (Early Jurassic) oceanic anoxic event in Yorkshire,  
802 UK. *Paleoceanography* 26, PA4210.

803 Kiessling, W., Simpson, C., 2011. On the potential for ocean acidification to be a general  
804 cause of ancient reef crises. *Glob. Change Biol.* 17, 56–67.

805 Killops, S.D., Massoud, M.S., 1992. Polycyclic aromatic hydrocarbons of pyrolytic  
806 origin in ancient sediments: evidence for Jurassic vegetation fires. *Org. Geochem.* 18,  
807 1–7.

808 Köster, J., van Kaam-Peters, H., Koopmans, M., de Leeuw, J., Sinninghe Damsté, J.,  
809 1997. Sulphurisation of homohopaneoids: Effects on carbon number distribution,  
810 speciation, and 22S/22R epimer ratios. *Geochim. Cosmochim. Acta* 61, 2431–2452.

811 Kruge, M.A., Stankiewicz, B.A., Crelling, J.C., Montanari, A., Bensley, D.F., 1994.  
812 Fossil charcoal in Cretaceous-Tertiary boundary strata: Evidence for catastrophic  
813 firestorm and megawave. *Geochim. Cosmochim. Acta* 58, 1393–1397.

814 Kuypers, M.M.M., van Breugel, Y., Schouten, S., Erba, E., Sinninghe Damsté, J.S., 2004.  
815 N<sub>2</sub>-fixing cyanobacteria supplied nutrient N for Cretaceous oceanic anoxic events.  
816 *Geology* 32, 853.

817 Lentz, S.J., Fewings, M.R., 2012. The Wind- and Wave-Driven Inner-Shelf Circulation.  
818 *Annu. Rev. Marine. Sci.* 4, 317–343.

819 Luo, G., Wang, Y., Algeo, T.J., Kump, L.R., Bai, X., Yang, H., Yao, L., Xie, S., 2011.  
820 Enhanced nitrogen fixation in the immediate aftermath of the latest Permian marine  
821 mass extinction. *Geology* 39, 647–650.

822 Macquaker, J., Bentley, S.J., Bohacs, K.M., 2010. Wave-enhanced sediment-gravity  
823 flows and mud dispersal across continental shelves: Reappraising sediment transport

824 processes operating in ancient mudstone successions. *Geology* 38, 947-950.

825 Macquaker, J., Taylor, K., 1996. A sequence stratigraphic interpretation of a mudstone-

826 dominated succession: the Lower Jurassic Cleveland Ironstone Formation. *J. Geol.*

827 *Soc. (London)* 153, 759-770.

828 Marynowski, L., Simoneit, B.R.T., 2009. Widespread Upper Triassic to Lower Jurassic

829 wildfire records from Poland: Evidence from charcoal and pyrolytic polycyclic

830 aromatic hydrocarbons. *Palaios* 24, 285-298.

831 McElwain, J.C., Wade-Murphy, J., Hesselbo, S.P., 2005. Changes in carbon dioxide

832 during an oceanic anoxic event linked to intrusion into Gondwana coals. *Nature* 435,

833 479-482.

834 Meyer, K.M., Macalady, J.L., Fulton, J.M., Kump, L.R., Schaperdoth, I., Freeman, K.H.,

835 2011. Carotenoid biomarkers as an imperfect reflection of the anoxygenic

836 phototrophic community in meromictic Fayetteville Green Lake. *Geobiol.* 9, 321-

837 329.

838 Moldowan, J.M., Sundararaman, P., Schoell, M., 1986. Sensitivity of biomarker

839 properties to depositional environment and/or source input in the Lower Toarcian of

840 SW-Germany. *Org. Geochem.* 10, 915-926.

841 Moldowan, J.M., Seifert, W.K., Gallegos, E.J., 1985. Relationship Between Petroleum

842 Composition and Depositional Environment of Petroleum Source Rocks. *Am. Assoc.*

843 *Petr. Geol. B.* 69, 1255-1268.

844 Naeher, S., Geraga, M., Papatheodorou, G., Ferentinos, G., Kaberi, H., Schubert, C. J.,

845 2012. Environmental variations in a semi-enclosed embayment (Amvrakikos Gulf,

846 Greece)- reconstructions based on benthic foraminifera abundance and lipid

847 biomarker pattern. *Biogeosciences* 9, 5081-5094.

848 Naqvi, S., Naik, H., Pratihary, A., D'Souza, W., Narvekar, P., Jayakumar, D., Devol, A.,

849 Yoshinari, T., Saino, T., 2006. Coastal versus open-ocean denitrification in the

850 Arabian Sea. *Biogeosciences* 3, 621-633.

851 Noble, R.A., Alexander, R., Kagi, R.I., Knox, J., 1986. Identification of some diterpenoid

852 hydrocarbons in petroleum. *Org. Geochem.* 10, 825-829.

853 O'Brien, N., 1990. Significance of lamination in Toarcian (Lower Jurassic) shales from

854 Yorkshire, Great Britain. *Sediment. Geol.* 67, 25-34.

855 Pálffy, J., Smith, P., 2000. Synchrony between Early Jurassic extinction, oceanic anoxic

856 event, and the Karoo-Ferrar flood basalt volcanism. *Geology* 28, 747-750.

857 Pancost, R., Crawford, N., Magness, S., Turner, A., Jenkyns, H., Maxwell, J., 2004.

858 Further evidence for the development of photic-zone euxinic conditions during

859 Mesozoic oceanic anoxic events. *J. Geol. Soc. (London)* 161, 353-364.

860 Pancost, R., Freeman, K., Patzkowsky, M., 1999. Organic-matter source variation and the

861 expression of a late Middle Ordovician carbon isotope excursion. *Geology* 27, 1015-

862 1018.

863 Peters, K.E., Walters, C.C., Moldowan, J.M., 2005. *The Biomarker Guide: Biomarkers*

864 *and Isotopes In Petroleum Systems and Earth History*, 2nd ed, *The Biomarker Guide:*

865 *Biomarkers and Isotopes in Petroleum Systems and Earth History.* Cambridge

866 University Press.

867 Powell, J.H., 2010. Jurassic sedimentation in the Cleveland Basin: a review. *Proc. Yorks.*

868 *Geol. Soc.* 58, 21-72.

869 Prauss, M., Ligouis, B., Luterbacher, H., 1991. Organic matter and palynomorphs in the

870 “Posidonienschiefer” (Toarcian, Lower Jurassic) of southern Germany. *Geol. Soc.,*  
871 *London Spec. Publ.* 58, 335–351.

872 Rashby, S., Sessions, A.L., Summons, R.E., Newman, D., 2007. Biosynthesis of 2-  
873 methylbacteriohopanepolyols by an anoxygenic phototroph. *Proc. Natl. Acad. Sci.*  
874 *U.S.A.* 104, 15099.

875 Röhl, H., Schmid, A., Oschmann, W., Frimmel, A., Schwark, L., 2001. The Posidonia  
876 Shale (Lower Toarcian) of SW-Germany: an oxygen-depleted ecosystem controlled  
877 by sea level and palaeoclimate. *Palaeogeogr. Palaeoclimatol. Palaeoecol.* 165, 27–52.

878 Sabatino, N., Neri, R., Bellanca, A., Jenkyns, H.C., Baudin, F., Parisi, G., Masetti, D.,  
879 2009. Carbon-isotope records of the Early Jurassic (Toarcian) oceanic anoxic event  
880 from the Valdorbia (Umbria-Marche Apennines) and Monte Mangart (Julian Alps)  
881 sections: palaeoceanographic and stratigraphic implications. *Sedimentology* 56,  
882 1307–1328.

883 Sãenz, J.P., Eglinton, T.I., Summons, R.E., 2011. Abundance and structural diversity of  
884 bacteriohopanepolyols in suspended particulate matter along a river to ocean transect.  
885 *Org. Geochem.* 42, 774–780.

886 Schlanger, S.O., Jenkyns, H.C., 1976. Cretaceous oceanic anoxic events: causes and  
887 consequences. *Geol. Mijnbouw* 55, 179–184.

888 Schouten, S., van Kaam-Peters, H., Rijpstra, W., Schoell, M., Sinninghe Damsté, J.,  
889 2000. Effects of an oceanic anoxic event on the stable carbon isotopic composition of  
890 Early Toarcian carbon. *Am. J. Sci.* 300, 1–22.

891 Schouten, S., Woltering, M., Rijpstra, W.I.C., Sluijs, A., Brinkhuis, H., Sinninghe  
892 Damsté, J.S., 2007. The Paleocene–Eocene carbon isotope excursion in higher plant  
893 organic matter: Differential fractionation of angiosperms and conifers in the Arctic.  
894 *Earth Planet. Sci. Lett.* 258, 581–592.

895 Schunck, H., Lavik, G., Desai, D.K., Großkopf, T., Kalvelage, T., Löscher, C.R.,  
896 Paulmier, A., Contreras, S., Siegel, H., Holtappels, M., Rosenstiel, P., Schilhabel,  
897 M.B., Graco, M., Schmitz, R.A., Kuypers, M.M.M., LaRoche, J., 2013. Giant  
898 Hydrogen Sulfide Plume in the Oxygen Minimum Zone off Peru Supports  
899 Chemolithoautotrophy. *PLoS One* 8, e68661.

900 Schwark, L., Frimmel, A., 2004. Chemostratigraphy of the Posidonia Black Shale, SW-  
901 Germany. *Chem. Geol.* 206, 231–248.

902 Sephton, M.A., Love, G.D., Meredith, W., Snape, C.E., Sun, C.-G., Watson, J.S., 2005.  
903 Hydropyrolysis: A new technique for the analysis of macromolecular material in  
904 meteorites. *Planet. Space Sci.* 53, 1280–1286.

905 Sepúlveda, J., Wendler, J., Leider, A., Kuss, H-J., Summons, R.E., Hinrichs, K-U., 2009.  
906 Molecular isotopic evidence of environmental and ecological changes across the  
907 Cenomanian–Turonian boundary in the Levant Platform of central Jordan. *Org.*  
908 *Geochem.* 40, 553–568.

909 Sinninghe Damsté, J.S., Schouten, S., Biological markers for anoxia in the photic zone of  
910 the water column. In: *The Handbook of Environmental Chemistry*, (Springer-Verlag,  
911 Berlin), pp. 127–163.

912 Sinninghe Damsté, J., Kenig, F., Koopmans, M., Köster, J., Schouten, S., Hayes, J., de  
913 Leeuw, J., 1995. Evidence for gammacerane as an indicator of water column  
914 stratification. *Geochim. Cosmochim. Acta* 59, 1895–1900.

915 Smith, F., Wing, S., Freeman, K., 2007. Magnitude of the carbon isotope excursion at the

916 Paleocene–Eocene thermal maximum: The role of plant community change. *Earth*  
917 *Planet. Sci. Lett.* 262, 50–65.

918 Smittenberg, R.H., Pancost, R.D., Hopmans, E.C., Paetzel, M., and Sinninghe Damsté,  
919 J.S., 2004. A 400-year record of environmental change in an euxinic fjord as revealed  
920 by the sedimentary biomarker record. *Palaeogeogr. Palaeoclimatol. Palaeoecol.* 202,  
921 331–351.

922 Stewart, F.J., Ulloa, O., DeLong, E.F., 2012. Microbial metatranscriptomics in a  
923 permanent marine oxygen minimum zone. *Environ. Microbiol.* 14, 23–40.

924 Suan, G., Nikitenko, B.L., Rogov, M.A., Baudin, F., Spangenberg, J.E., Knyazev, V.G.,  
925 Glinskikh, L.A., Goryacheva, A.A., Adatte, T., Riding, J.B., Föllmi, K.B., Pittet, B.,  
926 Mattioli, E., Lécuyer, C., 2011. Polar record of Early Jurassic massive carbon  
927 injection. *Earth Planet. Sci. Lett.* 312, 102–113.

928 Suan, G., Pittet, B., Bour, I., Mattioli, E., Duarte, L., Mailliot, S., 2008. Duration of the  
929 Early Toarcian carbon isotope excursion deduced from spectral analysis:  
930 Consequence for its possible causes. *Earth Planet. Sci. Lett.* 267, 666–679.

931 Summons, R.E., Jahnke, L., Hope, J., Logan, G., 1999. 2-Methylhopanoids as biomarkers  
932 for cyanobacterial oxygenic photosynthesis. *Nature* 23, 85–88.

933 Talbot, H., Farrimond, P., 2007. Bacterial populations recorded in diverse sedimentary  
934 biohopanoid distributions. *Org. Geochem.* 38, 1212–1225.

935 Talbot, H.M., Watson, D.F., Pearson, E.J., Farrimond, P., 2003. Diverse biohopanoid  
936 compositions of non-marine sediments. *Org. Geochem.* 34, 1353–1371.

937 Talbot, M., Livingstone, D., 1989. Hydrogen Index and Carbon Isotopes of Lacustrine  
938 Organic-Matter as Lake Level Indicators. *Palaeogeogr. Palaeoclimatol. Palaeoecol.*  
939 70, 121–137.

940 Tang, Y., Huang, Y., Ellis, G.S., Wang, Y., Kralert, P.G., Gillaizeau, B., Ma, Q., Hwang,  
941 R., 2005. A kinetic model for thermally induced hydrogen and carbon isotope  
942 fractionation of individual n-alkanes in crude oil. *Geochim. Cosmochim. Acta* 69,  
943 4505–4520.

944 ten Haven, H., Rohmer, M., Rullkötter, J., Bissert, P., 1989. Tetrahymanol, the most  
945 likely precursor of gammacerane, occurs ubiquitously in marine sediments. *Geochim.*  
946 *Cosmochim. Acta* 53, 3073–3079.

947 Trabucho-Alexandre, J., Dirx, R., Veld, H., Klaver, G., de Boer, P., 2012. Toarcian  
948 Black Shales in the Dutch Central Graben: Record of Energetic, Variable  
949 Depositional Conditions during an Oceanic Anoxic Event. *J. Sediment. Res.* 82, 104-  
950 120.

951 Trabucho-Alexandre, J., Tuenter, E., Henstra, G., van der Zwan, K., van de Wal, R.,  
952 Dijkstra, H., de Boer, P., 2010. The mid-Cretaceous North Atlantic nutrient trap:  
953 Black shales and OAEs. *Paleoceanography* 25, PA4201.

954 van Breugel, Y., Baas, M., Schouten, S., Mattioli, E., Sinninghe Damsté, J.S., 2006.  
955 Isorenieratane record in black shales from the Paris Basin, France: Constraints on  
956 recycling of respired CO<sub>2</sub> as a mechanism for negative carbon isotope shifts during  
957 the Toarcian oceanic anoxic event. *Paleoceanography* 21, PA4220.

958 van de Schootbrugge, B., McArthur, J.M., Bailey, T.R., Rosenthal, Y., Wright, J.D.,  
959 Miller, K.G., 2005. Toarcian oceanic anoxic event: An assessment of global causes  
960 using belemnite C isotope records. *Paleoceanography* 20, PA3008.

961 Venkatesan, M.I., Dahl, J., 1989. Organic geochemical evidence for global fires at the

962 Cretaceous/Tertiary boundary. *Nature* 338, 57–60.

963 Vetö, I., Demeny, A., Hertelendi, E., Hetenyi, M., 1997. Estimation of primary  
964 productivity in the Toarcia Tethys- a novel approach based on TOC, reduced sulphur  
965 and manganese contents. *Palaeogeogr. Palaeoclimatol. Palaeoecol.* 132, 355–371.

966 Wahlund, T., Woese, C., Castenholz, R., Madigan, M., 1991. A thermophilic green sulfur  
967 bacterium from New Zealand hot springs, *Chlorobium tepidum* sp. nov. *Arch.*  
968 *Microbiol.* 156, 81–90.

969 Wakeham, S., Schaffner, C., Giger, W., 1980. Polycyclic aromatic hydrocarbons in  
970 Recent lake sediments--I. Compounds having anthropogenic origins. *Geochim.*  
971 *Cosmochim. Acta* 44, 403–413.

972 Wakeham, S.G., Amann, R., Freeman, K.H., Hopmans, E.C., Jørgensen, B.B., Putnam,  
973 I.F., Schouten, S., Sinninghe Damsté, J.S., Talbot, H.M., Woebken, D., 2007.  
974 Microbial ecology of the stratified water column of the Black Sea as revealed by a  
975 comprehensive biomarker study. *Org. Geochem.* 38, 2070–2097.

976 Wakeham, S.G., Turich, C., Schubotz, F., Podlaska, A., Li, X., Varela, R., Astor, Y.,  
977 Sãenz, J.P., Rush, D., Sinninghe Damsté, J.S., Summons, R.E., Scranton, M.I.,  
978 Taylor, G. T., Hinrichs, K.-U., 2012. Biomarkers, chemistry, and microbiology show  
979 chemoautotrophy in a multilayer chemocline in the Cariaco Basin. *Deep-Sea Res. I*  
980 163, 133-156.

981 Wen, Z., Ruiyong, W., Radke, M., Qingyu, W., Guoying, S., Zhili, L., 2000. Retene in  
982 pyrolysates of algal and bacterial organic matter. *Org. Geochem.* 31, 757–762.

983 Wignall, P., Newton, R.J., Little, C.T.S., 2005. The timing of paleoenvironmental change  
984 and cause-and-effect relationships during the Early Jurassic mass extinction in  
985 Europe. *Am. J. Sci.* 305, 1014–1032.

986 Xie, S., Pancost, R., Yin, H., Wang, H., Evershed, R., 2005. Two episodes of microbial  
987 change coupled with Permo/Triassic faunal mass extinction. *Nature* 434, 494–497.

988 Zhang, C., Zhang, Y., Cai, C., 2011. Aromatic isoprenoids from the 25–65 Ma saline  
989 lacustrine formations in the western Qaidam Basin, NW China. *Org. Geochem.* 42,  
990 851-855.

991 Zundel, M., Rohmer, M., 1985. Prokaryotic triterpenoids. 1. 3 $\beta$ -Methylhopanoids from  
992 *Acetobacter* species and *Methylococcus capsulatus*. *Eur. J. Biochem.* 150, 23–27.

993

Figure 1

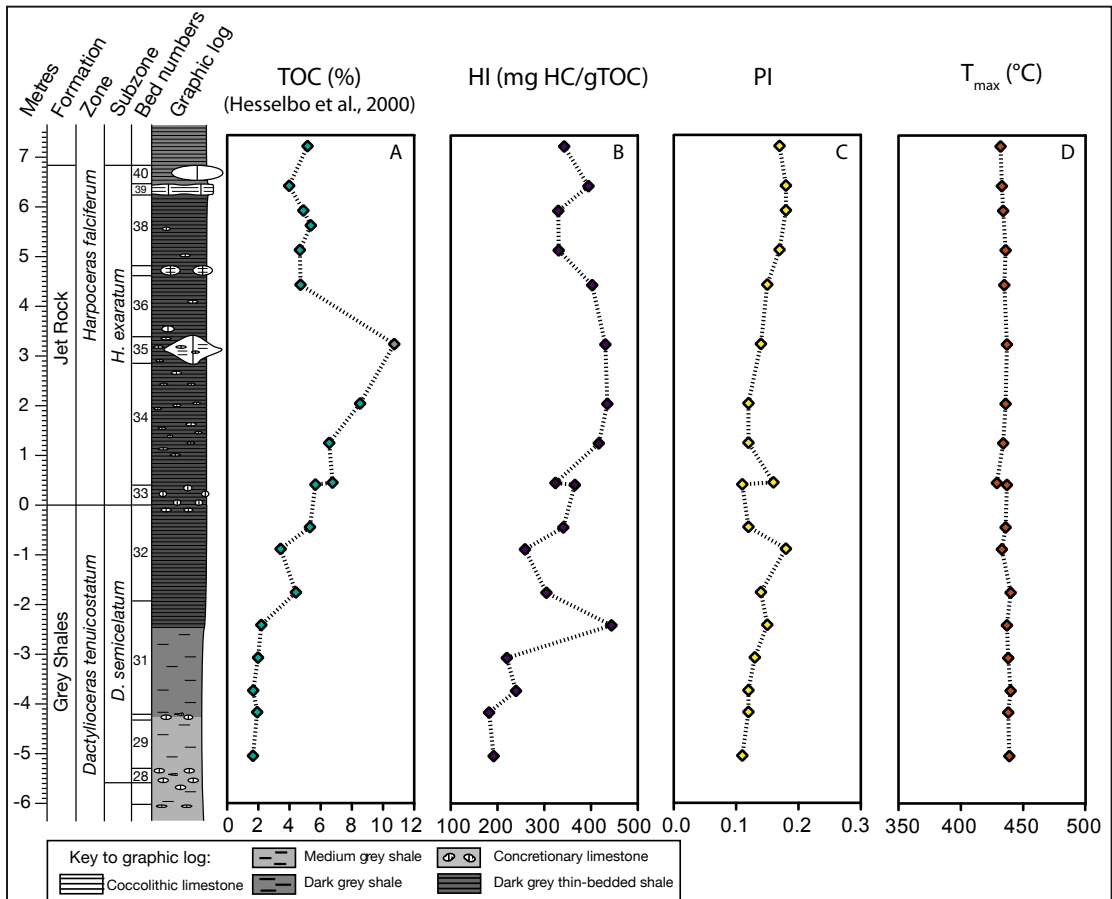


Figure 2

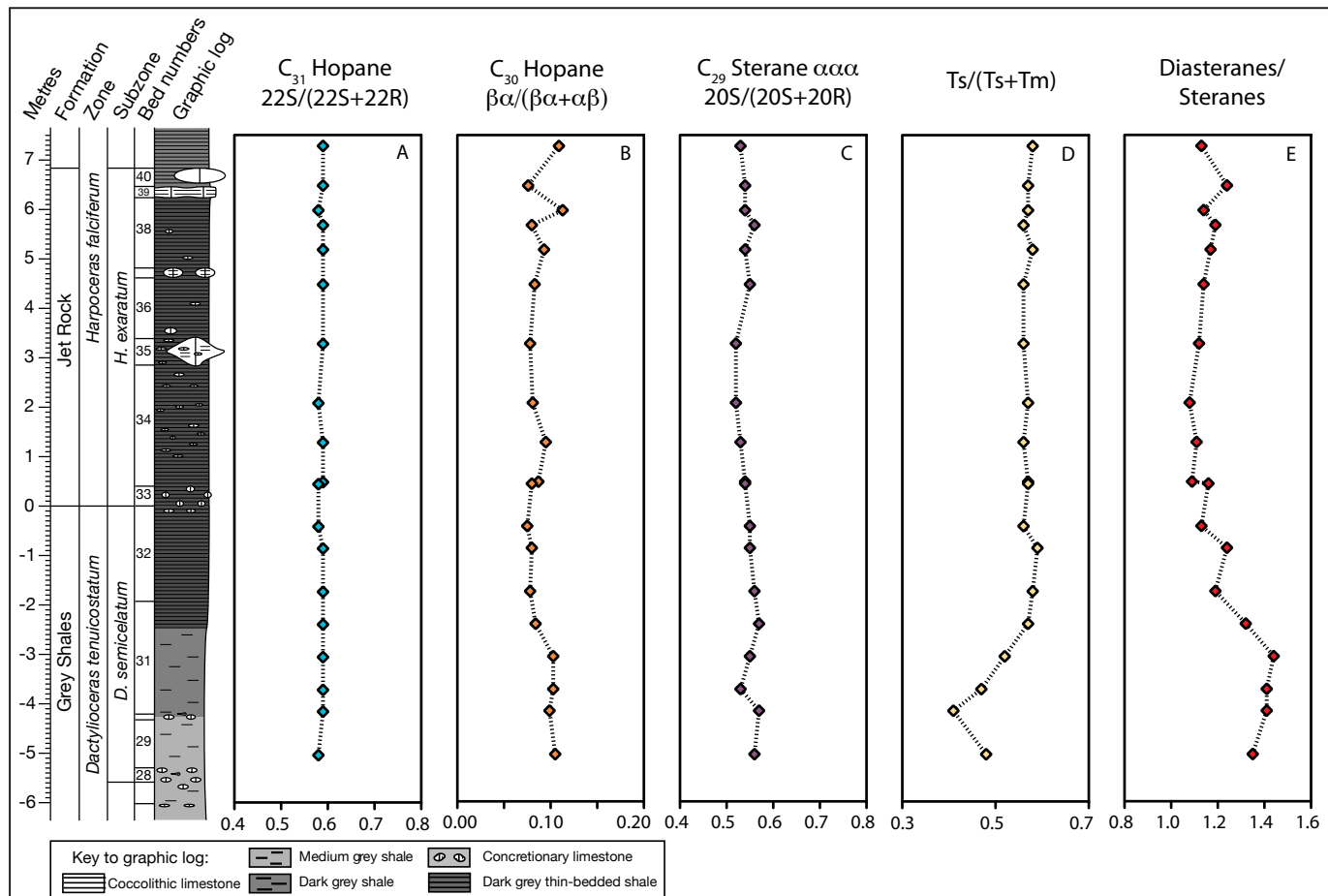


Figure 3

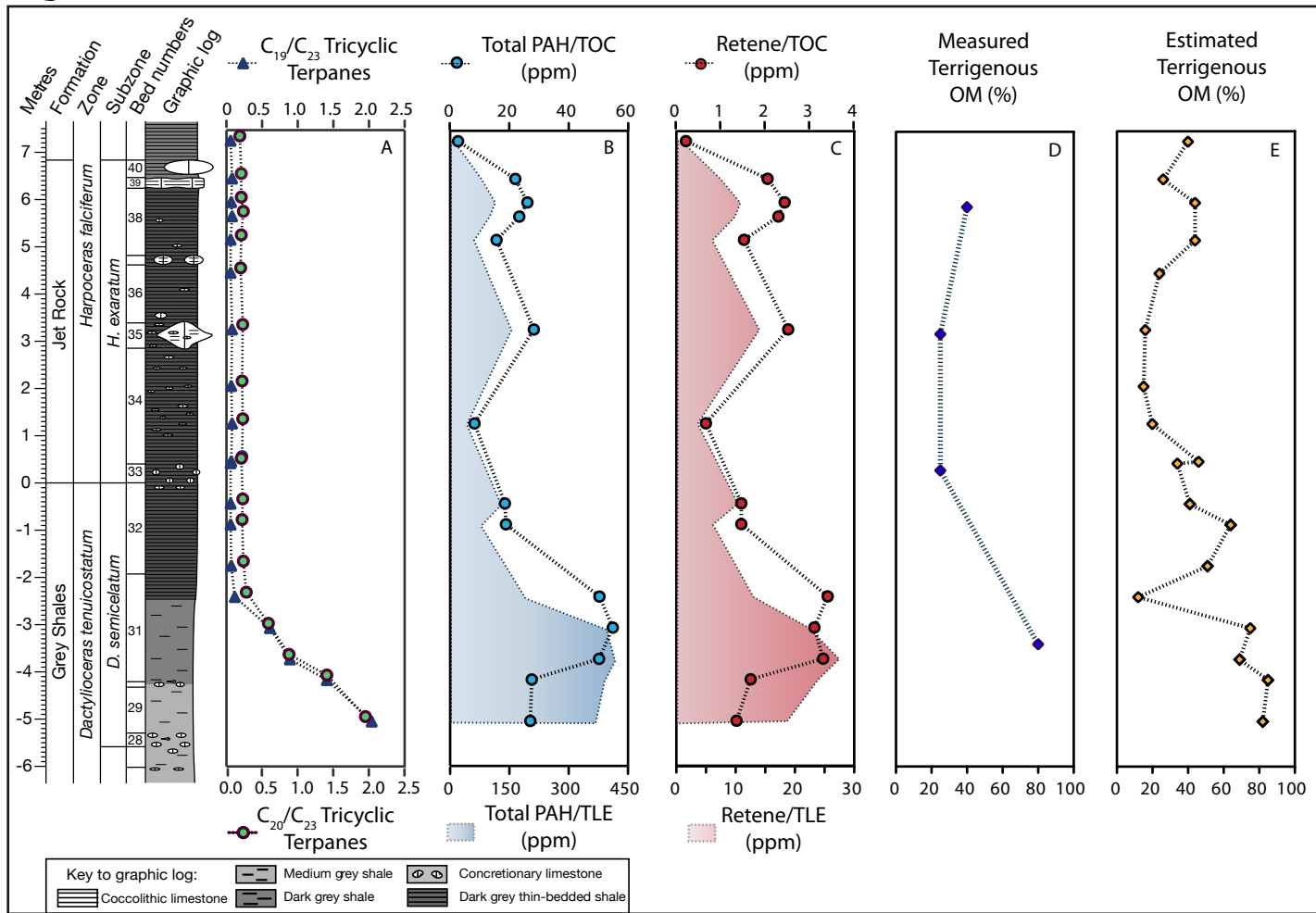




Figure 4

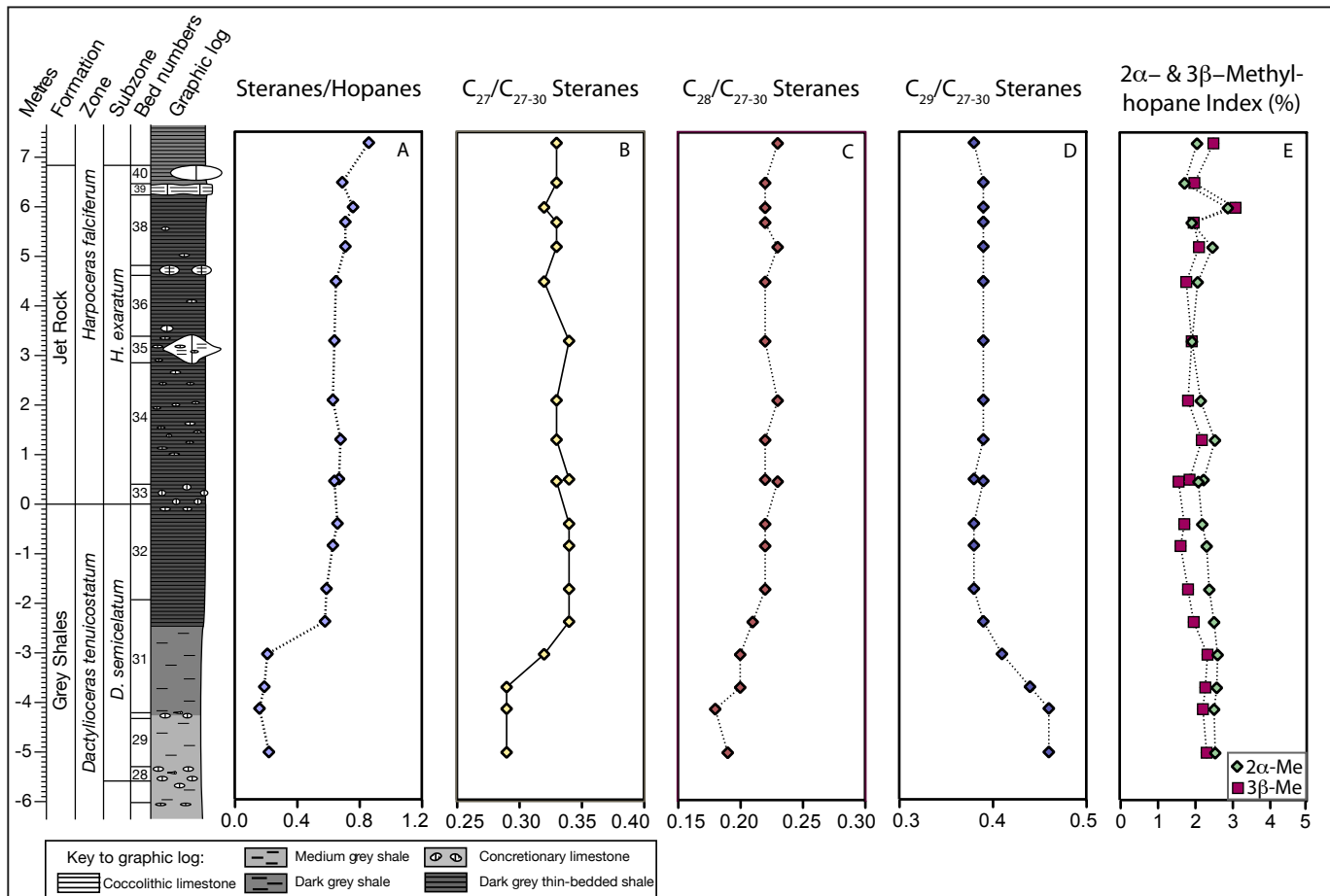


Figure 5

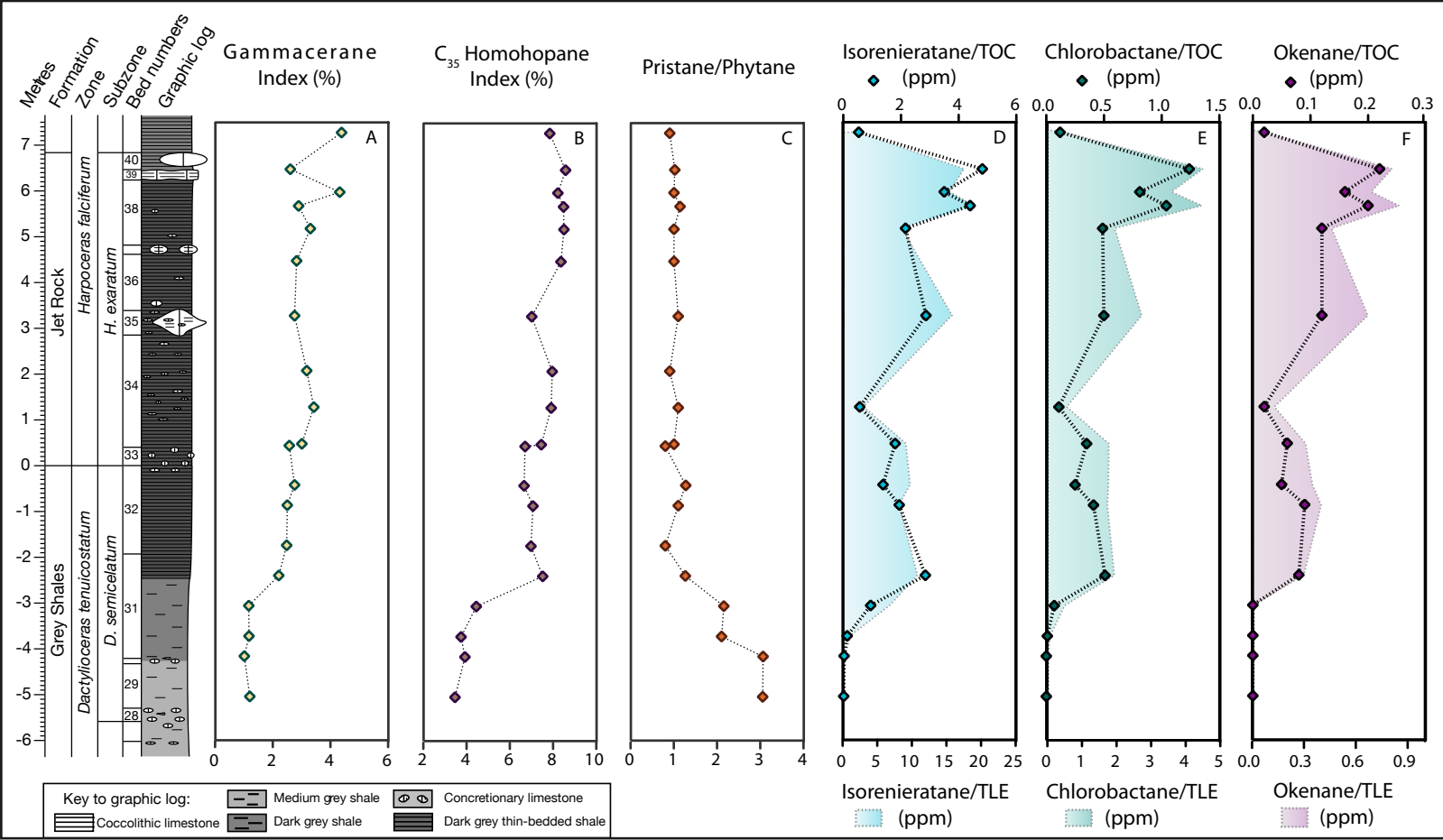


Figure 6

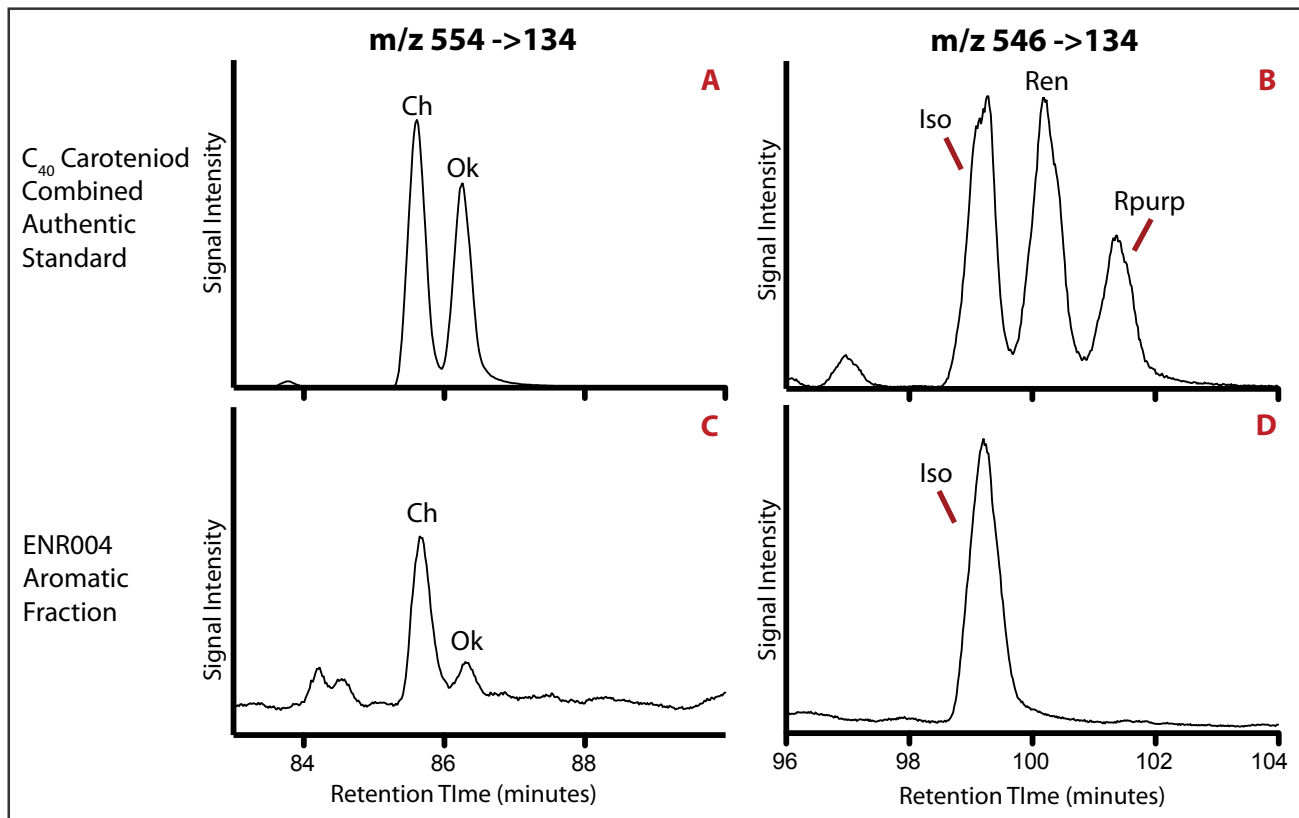
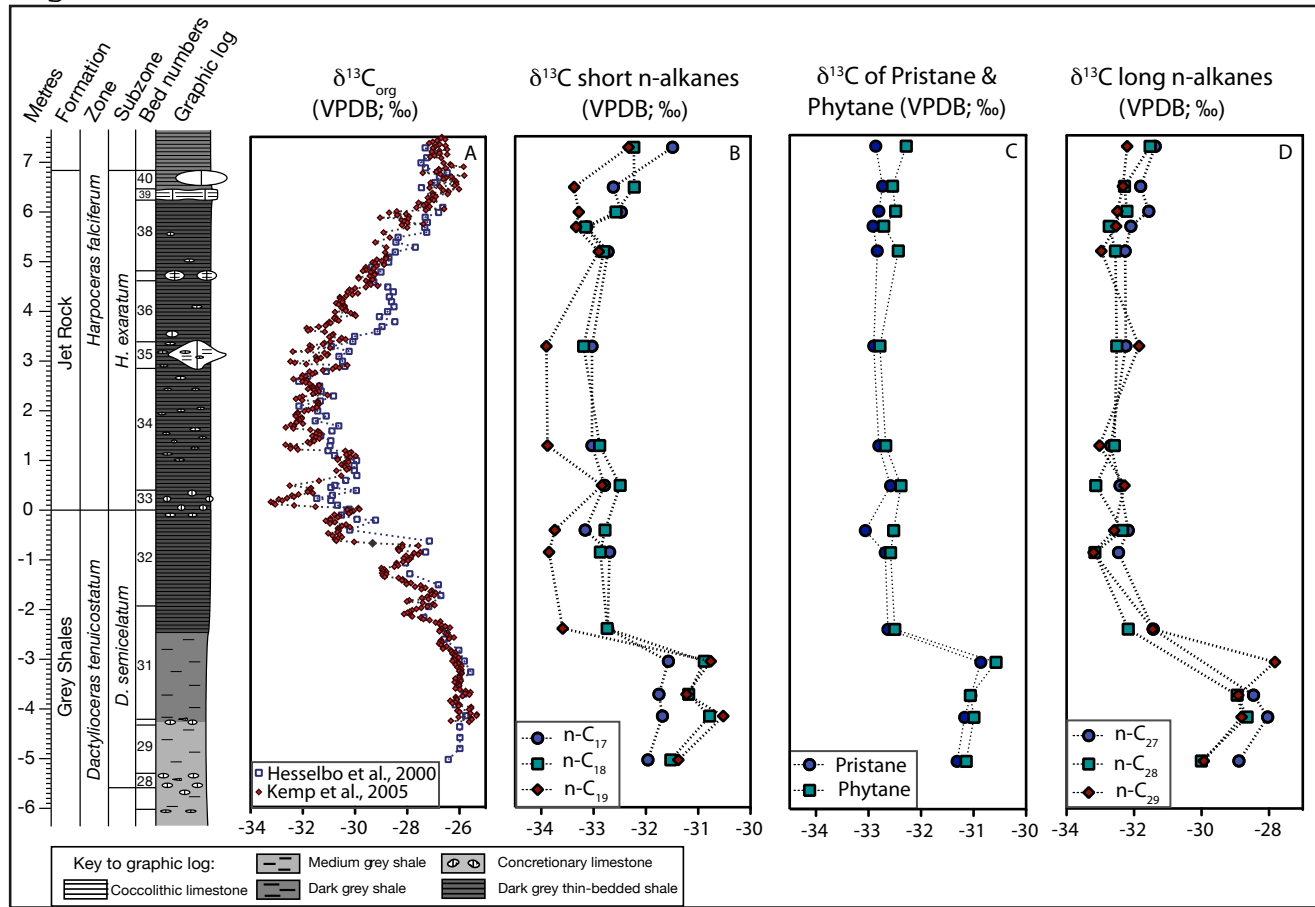


Figure 7



## Supplementary Online Material (SOM)

### *3.1 Rock-Eval pyrolysis*

Powdered sediment samples (~1 g) were analyzed at the University of Newcastle on a Rock-Eval pyrolysis instrument. The total organic carbon (TOC %),  $T_{\max}$  (°C),  $S_1$ , and  $S_2$  were determined. The  $S_1$  and  $S_2$  are expressed in mg hydrocarbons (HC) per gram dry rock. These parameters were used to calculate the hydrogen index (HI) ( $HI = [100 * S_2] / TOC$ ; expressed in mg hydrocarbon (HC)/g TOC) and the production index (PI) ( $PI = S_1 / [S_1 + S_2]$ ). The Rock-Eval TOC values and the bulk  $\delta^{13}C_{org}$  have been previously reported (Hesselbo et al., 2000).

### *3.2 Organic petrography*

In order to examine the nature of the organic matter, particularly the fraction of terrigenous organic matter, four samples across the section were prepared for optical analysis of the kerogen. Kerogen was isolated from the sample material remaining after lipid extraction as described in section 3.3. The mineral matrix was removed by the sequential addition of HCl and HF. Samples were centrifuged and rinsed between acid treatments, and the residual matter was rinsed with water and methanol. A subsample of each kerogen sample was mounted onto a slide in duplicate and assessed optically under white light and fluorescent light using a Zeiss research microscope and a Zeiss x 40 Plan-Neofluar objective. A Zeiss Axioskop, Axio Image D1, and a Zeiss 18 filter set were used to take photomicrographs and fluorescence images.

The fraction of terrigenous organic matter was estimated for the samples that were not analyzed by organic petrography using the linear relationship between the percent terrigenous organic matter measured by optical microscopy and the corresponding HI:

$$f_{Terr\ OM} (\%) = -0.279 * HI + 136 \quad (1)$$

where the linear regression had an  $R^2$  value of 0.90 and  $f_{Terr\ OM}$  represents the terrigenous organic matter as a percentage.

### 3.3 Biomarker extraction and analysis

Powdered samples (~ 5 g) were extracted using a Dionex ASE 200 Accelerated Solvent Extractor at 1000 psi and 100°C, with a solvent mixture of dichloromethane:methanol 9:1 (v/v). The total lipid extract (TLE) was reacted with acid-activated copper shots to remove elemental sulfur. Asphaltenes were separated (3x) from the maltene fraction by precipitation in n-pentane at 4°C, and after centrifugation at 3000 rpm for 10 minutes. The maltene fraction was then separated into saturated, aromatic, and polar fractions by silica gel chromatography using hexane, 1:1 (v/v) hexane/dichloromethane, and 7:3 (v/v) dichloromethane/methanol.

The saturated fractions were screened by gas chromatography-mass spectrometry (GC-MS) in full scan using an Agilent 6890 GC equipped with a HP6890 autosampler and interfaced to an Agilent 5973 mass spectrometer. Saturated hydrocarbons were also analyzed by gas chromatography-metastable reaction monitoring-mass spectrometry (GC-MRM-MS) on a Micromass Autospec Ultima mass spectrometer coupled with an Agilent 6890N GC. The analysis was carried out with a 60 m J&W Scientific DB-1 fused silica capillary column (internal diameter: 0.25 mm; 0.25 m film thickness) in pulsed splitless mode. The initial GC oven temperature was programmed to 60°C (held for 2

minutes), ramped to 150°C at 10°C/minute, and then to 315°C at 3°C/minute (held for 24 minutes). The ion source was in EI mode at a temperature of 250°C, an ionization energy of 70 eV, and acceleration voltage of 8000 kV. Tricyclic terpanes and hopanes were identified by MRM using the molecular ion to the m/z 191 transitions. Likewise, steranes were identified by MRM using the molecular ion to m/z 217 transitions.

The aromatic fraction was analyzed by GC-MS in SIM modes. Prior to analysis, 400 ng of an aromatic internal standard, deuterated phenanthrene, was added to each sample. The GC was fitted with a DB-5 stationary phase column, and the GC oven temperature was ramped from 60°C to 150°C at 20°C/minute, and then to 330°C at 4°C/minute (held for 27 minutes). The aryl isoprenoids and isorenieratane was identified in the m/z 134 ion chromatograms and quantified using the internal standard. Absolute quantification is not possible without taking into account relative response factors but our approach does allow an internally consistent estimation across the sample set.

The aromatic fraction was also analyzed by GC-MS in full scan and MRM modes on a Micromass Autospec Ultima mass spectrometer coupled with an Agilent 6890N GC autospec. The GC was fitted with a DB-5 stationary phase column. Polycyclic aromatic hydrocarbons (PAHs) were identified and quantified in full scan mode by their mass spectra and by comparison with a mix of authentic standards, with the exception of retene, coronene, and triphenylene, which were identified by their mass spectra and relative retention time. Aromatic carotenoid derivatives were also analyzed by GC-MRM-MS using parent-daughter reactions. Isorenieratane, okenane, and chlorobactane were identified in characteristic MRM transitions by comparison of retention times to an extract from the Barney Creek Formation (BCF) and a standard mix of hydrogenated

carotenoids containing chlorobactane, okenane, isorenieratane, renieratane, and renierapurpane. Using the MRM data, okenane and chlorobactane were quantified against the GC-MSD quantified isorenieratane. The aromatic carotenoid derivative and PAH concentrations were normalized against mass of TLE and TOC.

Compound specific carbon isotopic measurements of saturated hydrocarbons were made by gas chromatography/combustion/ isotope ratio mass spectrometry (GC-C-IRMS) using a Thermo Finnigan Delta plus XP coupled to a Thermo Finnigan Trace GC. The initial oven temperature was programmed to 60°C (held for 3 minutes), ramped to 180°C at 10°C/min, and then to 320°C at 4°C/min (held for 20 minutes). All samples were bracketed by pulses of in house calibrated reference CO<sub>2</sub> gas and Oztech calibrated reference CO<sub>2</sub> gas. A standard mix of *n*-alkanes (mix A; Arndt Schimmelmann, Indiana University) was analyzed twice a day to monitor the instrument condition. The mean value of triplicate analyses are reported here in permil (‰) relative to Vienna Pee Dee belemnite (VPDB), and the standard deviation from the mean value was better than 0.4‰.